國立中興大學機械工程學研究所

碩士學位論文

(初稿)

應用模擬分析與實驗設計法探討晶格支撐結構以最小化選擇性雷射熔融之熱變形

Study on the Lattice Support Structures to Minimize Thermal Distortion in Selective Laser Melting Using Simulation and Design of Experiments

指導教授: 莊俊融 Jyun-Rong Zhuang

研究生: 鍾沛栩 Pei-Hsu Chung

中華民國一一三年

摘要

選擇性雷射熔融(Selective laser melting, SLM)是一種建構複雜 3D 幾何模型的製造技術，由於其具備可製作複雜幾何工件與最小化材料浪費的優勢，故經常應用在人工關節植入物的製造中。晶格結構(Lattice structure)亦為保有結構剛性同時減少材料耗費的設計方式，因其複雜結構與 SLM 有良好的相性，故有作為支撐結構降低元件熱變形與殘留應力的潛力。然而現行研究大多探討晶格結構的剛性等機械性質，而缺少對其熱傳性能的探討。因此，需要提出方法以衡量晶格結構作為支撐結構時的熱傳能力。本研究旨在以實驗設計法(Design of Experiment, DOE)探討晶格支撐結構設計參數對 SLM 股骨元件熱效應的影響。首先，本研究提出單晶格夾層法(One-Lattice sandwich method)模擬其熱行為，並提出溫降時間與最高熱通量等量化指標以衡量晶格熱傳性能，結果發現 Octet 類型在簡單測試中具有最高剛性與最佳散熱能力。接著，為驗證晶格結構於複雜幾何上的性能，本研究將股骨元件之懸垂區域網格化以填入晶格單元作為支撐結構，透過改變晶格類型、尺寸與相對密度進行 FEM 模擬驗證，結果發現 Fluorite 類型在複雜幾何測試中具有最佳熱傳與降低熱變形的能力。最後，使用反應曲面法(Response Surface Methodology)探討晶格參數對 SLM 成品熱誤差的影響，結果發現降低支柱直徑、提升晶格尺寸可有效降低熱變形。

關鍵詞:選擇性雷射熔融、熱誤差、殘留應力、實驗設計法、支撐結構、晶格結構

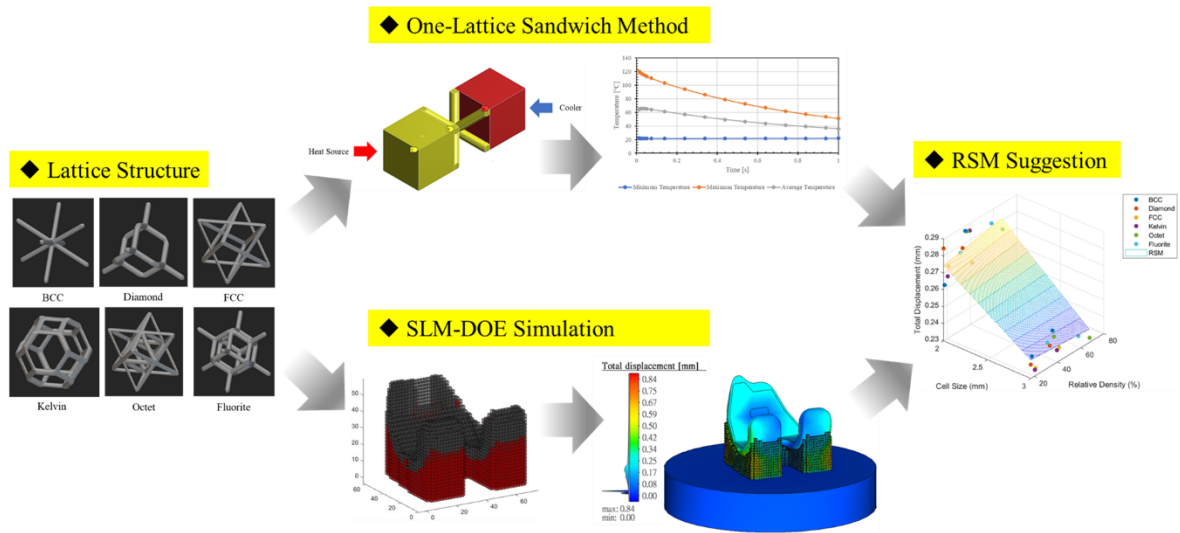# 圖摘要

Figure 1. Graphic abstract

Abstract

Selective Laser Melting (SLM) is a manufacturing technique for constructing complex 3D geometries, often used in producing artificial joint implants due to its ability to create intricate parts while minimizing material waste. Lattice structures, known for maintaining structural rigidity while reducing material usage, are highly compatible with SLM. They also have the potential as support structures to reduce thermal deformation and residual stress in components. However, current research primarily focused on the mechanical properties of lattice structures, with limited exploration of thermal conductivity. Therefore, it is necessary to develop a method to evaluate the thermal performance of lattice structures as support materials.

This study investigates the impact of lattice support structure design parameters on the thermal effects of SLM femoral components using the Design of Experiment (DOE). We introduce a One-Lattice Sandwich Method to simulate the thermal behavior of lattice structures, proposing metrics such as temperature drop time and maximum heat flux to quantify thermal performance. Our findings indicate that the Octet type lattice exhibits superior stiffness and heat dissipation performance under the simple geometry test. To validate the lattice structure's effectiveness on complex geometries, the overhanging regions of the femoral component are meshed and filled with lattice units as support structures. Through variations in lattice types, sizes, and relative densities, we identify that the Fluorite type lattice demonstrates the best heat dissipation and thermal displacement-minimizing capabilities under the complex geometry test. Finally, Response Surface Methodology (RSM) is utilized to analyze the effects of lattice parameters on the thermal accuracy of SLM-fabricated parts, revealing that reducing strut diameter and increasing cell size can minimize thermal displacement in femoral components.

Keywords: Selective Laser Melting; Thermal Displacement; Residual Stress; Design of Experiment; Supporting Structure; Lattice Structure

目錄

Introduction

1.1 Background

Since 2018, the proportion of people over 65 years old in Taiwan has exceeded 14% of the total population, symbolizing that Taiwan has officially entered an elderly society [1]. The issue of long-term care has attracted much attention, which has led to the booming development of related medical industries. One of these medical industries is total knee arthroplasty (TKA), which aims to replace worn-out old knee joints with artificial knee implants, enabling the elderly to regain mobility. According to statistics from the Health Promotion Administration [2], the prevalence rate of degenerative knee arthritis in Taiwan is about 15%, which means that 3.5 million people suffer from degenerative knee joint pain. However, on average, only about 20,000 knee joint replacements are performed yearly. The reason for the low rate of surgery is that patients have psychological fear of the surgery, worry about postoperative pain, recovery, and the risks of needing to be readmitted to the hospital for replacement, and even choose to make compromises such as enduring pain and reducing movement. Therefore, special attention needs to be paid to the manufacturing method and installation technology of artificial knee joints, so that the elderly can have more confidence in the success rate of artificial knee replacement.

Clinically, the key to the success of this operation lies in whether the three components of the artificial knee joint: the femoral metal sleeve, the tibial metal plate, and the plastic gasket are accurately installed on the native bone and can perform the functions of connection and movement [3], such as shown in Figure 2. Once the deviation between the native bone and the implant exceeds 1 mm [4], it will greatly affect the contact force and wear rate between joints, resulting in postoperative infection, pain, instability, and other sequelae. In recent years, with the improvement of medical and manufacturing technology, the proportion of patients requiring

readmission within one month after artificial knee replacement has been stably maintained at less than 0.4%, as shown in Figure 3. However, if artificial knee replacement is to be more reliable, advanced and sophisticated manufacturing methods are needed to increase patients' trust in the treatment.
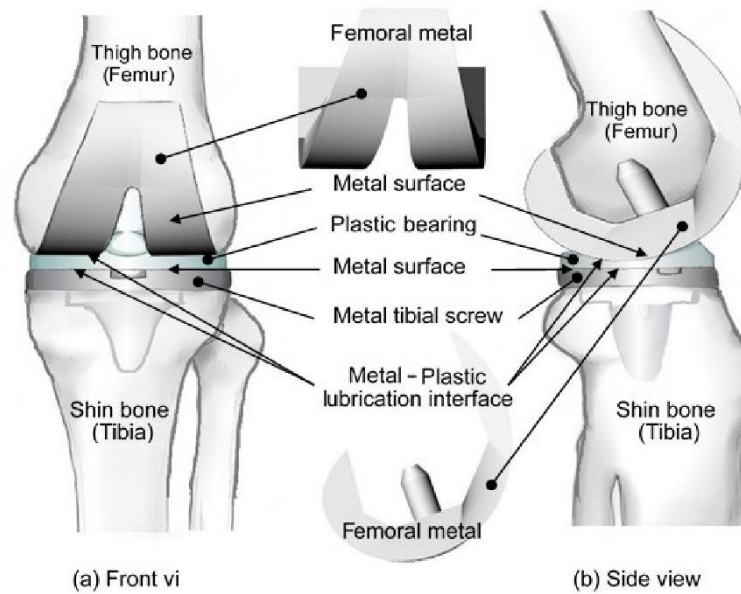

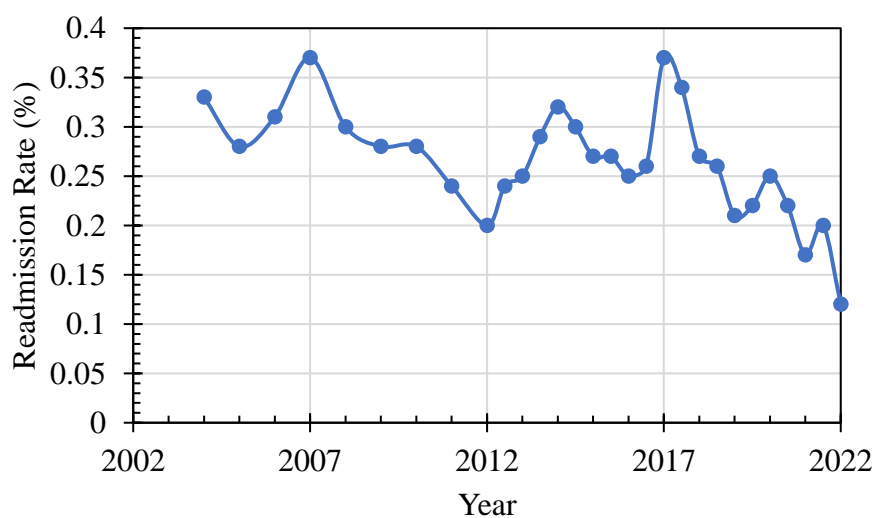Figure 2. Artificial knee joint front view and side view [3]

Figure 3. Trend chart of readmission rate due to related problems within 30 days after

discharge from artificial knee replacement surgery [2]

Literature Review

In the past decade, additive manufacturing (AM) has attracted widespread attention from the industry due to its ability to manufacture complex geometric parts [5]. Compared with traditional manufacturing technologies (such as casting, milling, etc.), it can break through its manufacturing limitations and produce parts with a high degree of freedom based on computer-aided technology (CAD). Especially in the context of Industry 4.0, additive manufacturing technology can help manufacturers minimize the waste of materials and reduce costs while producing complex parts. Therefore, it is regarded as an environmentally friendly and sustainable technology. Metal additive manufacturing can be divided into four main technologies according to its manufacturing process: material extrusion, binder jetting, powder bed fusion, and directed energy deposition.

Among the above technologies, powder bed fusion is also called selective laser melting (SLM)[6]. The principle of this technology is to use laser light to heat metal powder scattered on the workbench to make the metal powder crystallize. Granular fusion constructs a complex three-dimensional geometric model in a layer-by-layer superposition manner [7], as shown in Figure 4. This technology is regarded as a processing method that can meet the precision requirements of artificial knee joints due to its ability to manufacture complex geometric components and minimize material waste. The complete process includes in sequence: inputting model files, detecting overhang areas, printing, heat treatment, cutting off the bottom plate, and removing the support structure, as shown in Figure 5. Although this technology can manufacture complex parts, it will produce high-temperature gradients during the layer-by-layer laser scanning process, which will lead to defects such as thermal deformation and residual stress [8]. In more serious cases, it can also lead to cracks, delamination, shrinkage, warping, and other failures in the finished product, so it is regarded as a key problem that needs to be overcome. The first solution is to improve the microstructure of the printed product

through heat treatment to achieve the goal of improving its mechanical properties [9]. However, post-processing requires additional costs and is not suitable for small factories without relevant equipment. The second method is to use a support structure to connect the parts to the base plate to provide mechanical tension to prevent deformation, warping, and other defects. However, the support structure requires additional materials, and the step of removing the support structure will also increase post-processing costs. The third way is to optimize the design of the workpiece itself, by incorporating limitations such as end-use performance into the boundary conditions, and then find the optimal geometry of the workpiece. However, some industries do not want to modify the original design of the workpiece. Based on the above, how to solve the problems of thermal deformation and residual stress while minimizing processing costs is currently a hot research direction.
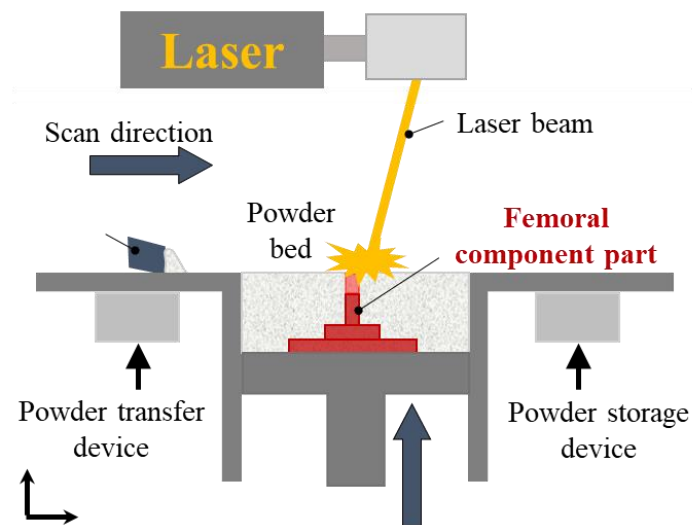

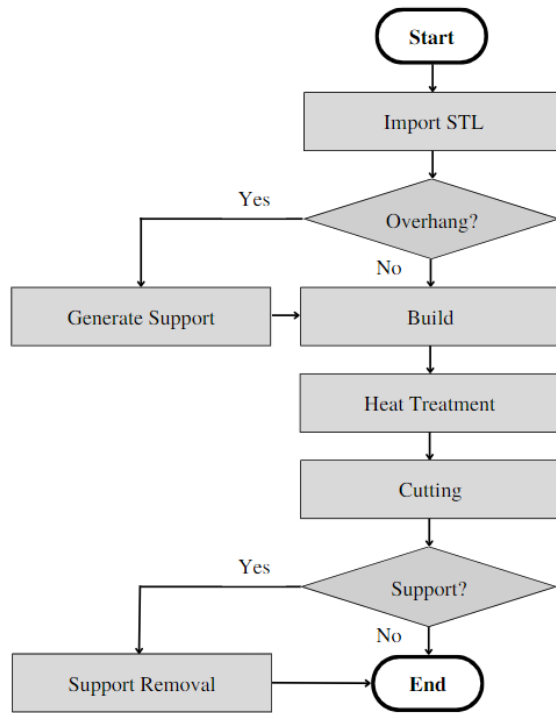Figure 4. Schematic diagram of SLM printing process [7]

Figure 5. SLM process [5]

2.1 Support Structures

The support structure design is one of the common preparations in metal additive manufacturing technology [10], which has four main functions: 1. Supporting overhang areas, holes, or bridges to achieve printability; 2. Maintaining stability during the printing process. Manufacturability of parts; 3. Facilitate removal from base plates and workpieces; 4. Assist thermal diffusion or prevent residual stress caused by laser melting during scanning.

To generate a support structure for a workpiece with a given build direction, there are two main steps: identifying the overhang area and generating a topology to connect the overhang area to the base plate [11]. In the research of Zhang et al.[12], it is believed that further analysis and optimization of overhang areas such as medical components that require complex structures are needed, and the overhang areas are subdivided into overhang surfaces, overhang edges, and

overhang points. Selecting support points is an extremely critical step in generating a support structure, as it will play a direct role in the deformation and thermal conductivity of the printed workpiece. Therefore, the mechanical properties of the support structure should be ensured first, and then the thermal effects should be included in the optimization process. Current methods for generating support structures include: 1. Direct projection-based method, which means projecting the overhang area onto the floor and generating linear thin walls with predefined cross-sectional profiles along the projection rays. Because of its simple operation, this method is adopted by many commercial software, as shown in Figure 6(1). 2. Lattice filling method [13], which means that in the projection-based method, predefined cellular lattice units are used instead of solid walls, which can form porous supports to reduce the amount of material, as shown in Figure 6(2). Venugopal et al.[26] proposed a multi-material topology optimization method for variable density lattice structures, which fills the lattice structure with predefined geometric shapes into the overhang area to minimize flexibility and improve heat transfer capabilities. 3. Tree-type supporting method [14], which means to generate a tree-like support structure through support cones and node generation rules. It can find the minimum cumulative path and the diameter is variable to ensure the stability of different branch layers, as shown in Figure 6(3). Subedi et al.[15] proposed a layer-by-layer tree support structure generation algorithm for LPBF. In addition to providing sufficient support force, they also conducted experiments to verify its effect in preventing thermal defects. However, this method is difficult to control and has high computational costs. If the efficiency of the topology optimization algorithm can be improved, it has the potential to become an algorithm that provides optimal design solutions for support structures. 4. Bridge-type supporting method [16], which means providing support with a columnar structure, considers the maximum lateral bridge length limit to further simplify the generation, as shown in Figure 6(4).
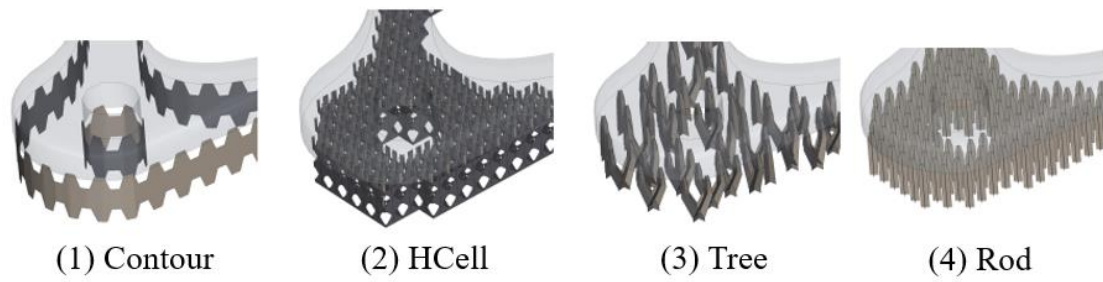
(1) Contour   (2) HCell   (3) Tree   (4) Rod

Figure 6. 4 major types of support structures [37]

2.2 Lattice Structure

Lattice structure has gradually received widespread attention in the precision industry because it can maintain important material capabilities such as rigidity, strength and durability while minimizing material consumption. The main method is to repeatedly arrange and fill predefined cells into parts to achieve lightweight materials and improve mechanical, acoustic and dielectric properties. Due to its complex and delicate geometry, this structure is difficult to fabricate using traditional methods and is therefore often used in conjunction with metal additive manufacturing techniques that can produce highly complex components. Lattice structures have been widely used in the aerospace, shipbuilding and medical industries. Armanfar et al.[17] embedded the lattice structure into the hull to improve the structural rigidity and reduce the weight of the hull. Longhitano et al.[18] designed various The pore size Ti6Al4V lattice structure is manufactured by PBF and tested for corrosion, wear and friction corrosion, and then the microstructure is observed to analyze the compatibility of the sample in orthopedics. However, the porosity, dimensional errors and microstructural defects produced by the lattice structure during the SLM process may have a negative impact on the lattice performance, such as reducing strength, rigidity and durability. Optimization of SLM process parameters can reduce the above defects, but due to the complexity of the thermo-solid coupling effect of the process itself, these defects are inherent to a certain extent. Therefore, how to

design the geometry of the lattice structure according to the target specifications is an important issue to ensure performance and prevent defects.

Many scholars have proposed methods to design and monitor lattice structures to improve the mechanical properties of the lattice and prevent defects. Han et al.[19] used μCT scanning to analyze the effects of lattice type, size, and relative density on porosity and dimensional errors. However, important mechanical properties such as rigidity and vibration resistance cannot be verified by scanning image data alone. Xu et al.[20] optimized the parameters of the lattice structure to adapt to the manufacturing of reinforced fiber laminates. However, the goal of parameter optimization was to improve the structural rigidity and did not discuss the heat transfer performance. Wang et al.[21] proposed a topology optimization formula to generate a 3D printing lattice support structure, which improves rigidity while ensuring self-support and manufacturability. However, its self-support is limited to numerical errors in the algorithm that may destroy self-support. properties, and no mention of heat transfer capabilities. Huang et al.[22] proposed a lattice-tree composite support structure generation algorithm to meet the manufacturing needs of parts with complex geometric shapes. However, their algorithm did not consider the possibility that edges are prone to warping due to residual stress caused by thermal gradients, and lattice structure and overhang identification contribute to the complexity of the algorithm. Yang et al.[23] designed a self-supporting BCC lattice and filled it into the optical mirror as a supporting structure to provide rigidity, and vibration resistance and reduce the overall weight. At the same time, they proposed a coordinate conversion equation to adapt to the surface definition domain. However, they present that changes in lattice shape after label conversion may destroy self-supporting properties, and heat transfer capabilities are not considered. Vaidya et al.[24] applied Dijkstra's shortest path algorithm to fill solid or hollow lattices to reduce the support volume and contact area, but the manufacturability and rigidity of their structure have not been experimentally verified. Liu et al.[25] proposed a stress-driven

9

multi-agent system conformal lattice filling strategy, which can increase the rigidity by 1.4 times compared with traditional lattice while considering manufacturability. However, the use of response surface methodology to accelerate performance evaluation may cause numerical errors and does not take into account the thermal behavior of the lattice. Venugopal et al.[26] proposed a multi-material topological optimization interpolation method to generate a lattice structure, and can simultaneously consider flexibility and thermal flexibility as the objective function. However, numerical testing is only carried out in the rectangular design domain, which has not yet been able to adapt to complex geometric components in practical applications.

2.3 Summary of literature review

Although there have been many studies on support structure generation methods and lattice structures, their limitations are as follows:

1. Most of them only discuss how to produce a self-supporting geometric structure in a given area, such as mechanical properties such as rigidity, strength, and vibration resistance, but less attention is paid to thermal transfer properties such as temperature, heat flux, and thermal deformation.

2. Most methods of monitoring lattice structure require compression testing and CT scanning to evaluate mechanical properties such as rigidity and porosity. However, due to the microscopic complexity of the lattice itself, there is a lack of methods to predict lattice properties in a low-cost way through numerical simulation.

3. Many literatures use topological optimization methods to modify the lattice to apply to complex geometric structures. However, this type of algorithm is computationally expensive and easily destroys the original self-supporting properties of the lattice.

Based on the above reasons, how to find index factors to evaluate the thermal behavior of lattice structures and generate lattice support structures in SLM that can minimize thermal

deformation of finished products while ensuring their self-supporting properties for various complex geometric components. This is a research question currently to be solved.

2.4 Research purpose

This study aims to reduce the thermal deformation of SLM femoral components with the lattice structure. First, the One-Lattice sandwich method is proposed to simulate the thermal behavior of the lattice. Six types of lattices were generated through nTopology [27], and quantitative metrics such as temperature drop time and maximum heat flux were proposed to measure heat transfer performance. Next, this study applied the Design of Experiments (DOE) [28] to verify the thermal behavior of the lattice structure on complex geometry, voxelizing the overhang area of the femoral component to fill in the lattice units as the support structure. Finite element method (FEM) simulation verification was performed by changing the lattice type, size, and relative density to explore the impact of lattice design parameters on the thermal deformation of the finished SLM product.

2.5 Research originality and contribution

The originality of this research is as follows:

1. There are few studies on the heat transfer performance of lattice structures, so this study proposes the One-Lattice sandwich test to simulate and verify its thermal behavior.

2. There are few studies on the thermal behavior of lattice as an SLM support structure. Therefore, this study uses simple geometric elements to test the influence of lattice type on thermal deformation and thermal stress of horizontal planes, inclined planes, and arc surfaces.

3. Few studies have discussed the impact of lattice structure on thermal deformation of

finished SLM products. Therefore, this study uses the full factorial design method to propose the optimal design parameters that can reduce the thermal deformation of femoral components.

The contributions of this study are as follows:

1. Propose a quantitative index of heat transfer to evaluate the performance of the lattice structure.

2. Propose the thermal effects when the lattice structure is applied to different geometric structures and the optimal lattice type selection.

3. Propose the design parameters of the lattice support structure that can minimize the thermal deformation of the finished SLM product.

Methodology

Lattice structure originally described the phenomenon of repeated symmetrical arrangements of atoms, molecules, or ions in nature, and has been widely studied in the fields of chemistry, biology, and materials [29]. In recent years, lattice structures have been widely favored in the industrial field because they can minimize material consumption while maintaining mechanical properties such as rigidity and strength, and are gradually being used in the aerospace and medical industries. Lattice structures are also potential candidates for heat exchangers due to their high surface area-to-volume ratio [30]. However, most of the past research on lattice structures discussed mechanical properties such as rigidity and compression energy absorption. There is a lack of unified measurement metrics for the heat transfer performance of lattice structures. In addition, although much literature has proposed SLM support structure optimization algorithms, there are few studies on the impact of support structure design parameters on the thermal behavior of finished products. Therefore, this study proposes an optimization method for lattice structure design to measure its thermal effect and heat transfer capability in the SLM process. The process is shown in Figure 7 and is summarized as follows:

1. This study proposes the One-Lattice sandwich method, which means using a single lattice structure as the barrier between two splints and giving a given temperature difference on both sides. The heat exchange behavior of the system is simulated through FEM, and two metrics, temperature drop time and maximum heat flux are defined to quantify the heat transfer performance of the lattice unit.

2. This study uses a simple geometry test to test the thermal effect of the lattice as an SLM support structure using simple geometric elements. By designing three geometric structures: cube, triangular prism, and arc surface, and applying different lattice support structures in sequence, the impact of lattice types on the total

deformation and thermal stress of horizontal planes, inclined planes, and arc surfaces was explored.

3. This study uses full factorial design to explore the thermal effects of lattice structure design parameters. By using the lattice structure as the support structure of the femoral component in SLM, the effects of lattice type, cell size, and strut diameter on the thermal deformation and residual stress of the finished femoral component were analyzed.

Through the above method, this study is expected to propose a quantitative index of the heat transfer performance of the lattice structure, so that processing personnel can efficiently evaluate the thermal effect of the SLM support structure and select the optimal design parameters.
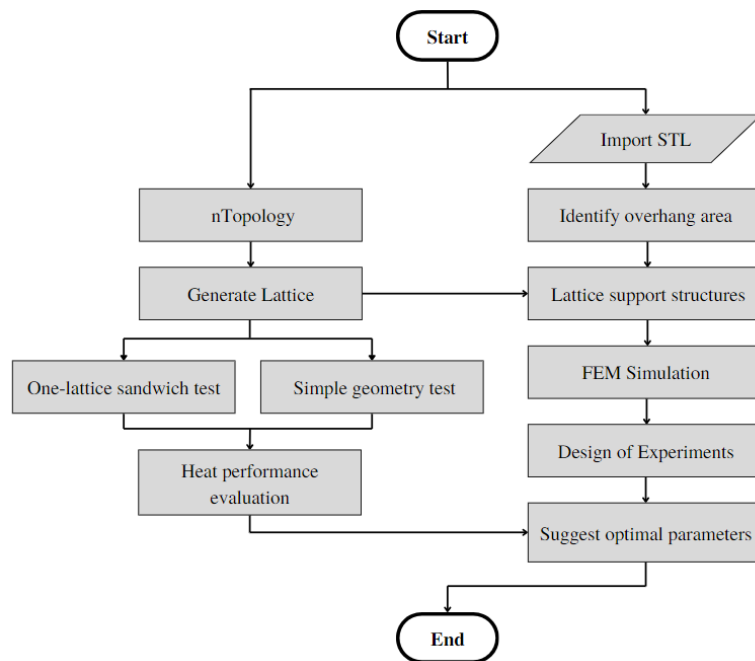
Figure 7. Lattice structure design parameter optimization flowchart

3.1 One-lattice sandwich method

The most common application method of lattice structures is to fill the interior of large structures to maintain rigidity while reducing the weight of the material, such as in the bulkheads of aircraft or ships. However, this type of application method often faces the situation of inconsistent environments on both sides of the partition, such as the temperature difference and pressure difference between the inside and outside of the cabin when the aircraft is at high altitude. Although there have been studies to evaluate the heat exchange behavior of the lattice structure in this case [31], current research still lacks a unified index to evaluate the heat transfer performance of the lattice structure. Therefore, this study proposes the One-Lattice sandwich method to evaluate the heat transfer performance of the lattice structure, which means sandwiching the single lattice structure between two partitions and applying different boundary conditions on both sides to simulate the actual situation.

The classic heat conduction formula is shown in Equation (3-1):

$$\dot{Q} = kA\frac{\Delta T}{d} \qquad (\text{ 3-1 })$$

where $\dot{Q}$ is heat flux (W); k is the thermal conductivity coefficient (W/m·K); A is the cross-sectional area of an object (m^2); ΔT is the temperature difference between two sides of the object (K); d is the thickness of the object (m).

The heat exchange capacity of the lattice structure comes from its high surface area to volume ratio, so the heat convection phenomenon on its surface must also be considered. The classic thermal convection formula is shown in Equation (3-2):

$$\dot{Q} = hA(T - T_f) \qquad (\text{ 3-2 })$$

where $\dot{Q}$ is heat flux (W); h is the thermal convection coefficient (W/m^2·K); A is the surface area of the object (m^2); T is the surface temperature of the object (K); T_f is fluid temperature (K).

This study uses Ansys 2020 R1 to perform simulation tests. The boundary conditions are as follows: Set a single cubic lattice size of 1 mm, with solid cubes of 1 mm³ on both sides to sandwich the lattice. One of the cubes is maintained at a normal temperature of 22°C as the cooling end, and the other cube is given an initial temperature of 122°C as the heat source, the material is 316L Steel, and the thermal convection coefficient is 12.1 W/m²·K [32]. The overall setup is shown in Figure 8. In addition, a compression test was also simulated to test the rigidity of a single lattice. The boundary condition was that one side of the lattice was fixed and the other side was given a displacement of 0.1 mm [33]. After obtaining the reaction force of the compression surface, Hooke's law can be used to calculate the rigidity of the single lattice. The overall setup is shown in Figure 9.
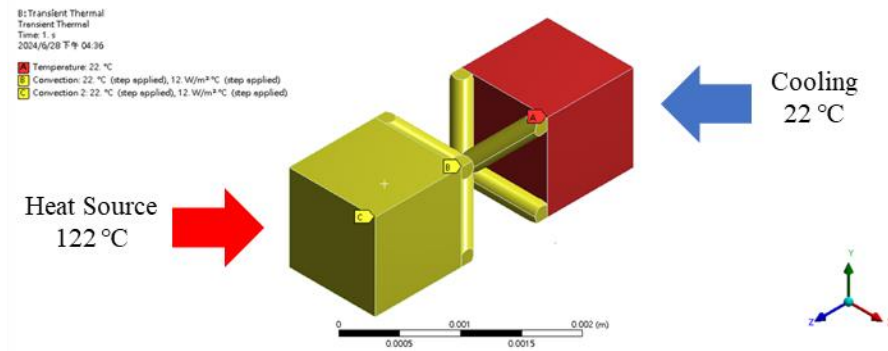
Figure 8. Single lattice heat transfer test boundary conditions
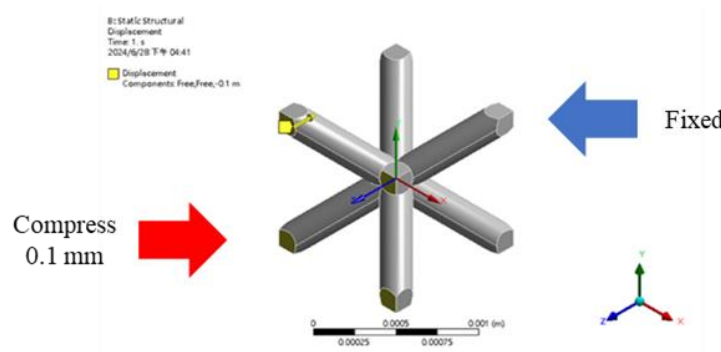
Figure 9. Single lattice stiffness test boundary conditions

Single lattice stiffness is obtained through compression tests and Hooke's Law:

$$\mathbf{F} = \mathbf{KU} \qquad (3\text{-}3)$$

where $\mathbf{F}$ is the force vector (N); $\mathbf{K}$ is the stiffness matrix (N/mm); $\mathbf{U}$ is the displacement vector (mm).

In order to define a quantitative index of the heat transfer performance of a single crystal lattice, this study describes the thermal behavior of the object from the basic heat conduction equation [34]. Consider the three-dimensional temperature equation over time of an object that generates heat (3-4):

$$\frac{1}{\alpha}\frac{\partial T}{\partial t} = \left(\frac{\partial^2 T}{\partial x^2} + \frac{\partial^2 T}{\partial y^2} + \frac{\partial^2 T}{\partial z^2}\right) + \frac{1}{k}q, \quad \alpha = \frac{k}{c\rho} \qquad (3\text{-}4)$$

where T is temperature (K); q is the heat generated per unit volume of an object (W/m^3); α is the thermal diffusion coefficient (m^2/s); k is the thermal conductivity coefficient (W/m·K); c is heat capacity (J/K); ρ is density (kg/ m^3).

If the object does not generate heat, Equation (3-4) can be rewritten as:

$$\frac{\partial T}{\partial t} = \alpha\nabla^2 T = \alpha\left(\frac{\partial^2 T}{\partial x^2} + \frac{\partial^2 T}{\partial y^2} + \frac{\partial^2 T}{\partial z^2}\right) \qquad (3\text{-}5)$$

We can solve the temperature equation using the separation of variables method:

$$u(x,t) = X(x)T(t) \qquad (3\text{-}6)$$

$$\frac{T'(t)}{\alpha T(t)} = \frac{X''(x)}{X(x)} = -\lambda \qquad (3\text{-}7)$$

where λ is a constant given for solving ordinary differential equations. When $\lambda > 0$, The solution to the equation of temperature decrease with time is shown in Equation (3-8):

$$T(t) = C - Ae^{-\lambda\alpha t} = C - A(\frac{1}{2})^{-\frac{t}{\eta}} \qquad (3\text{-}8)$$

When the location and initial conditions of the heat source are known, the heat equation can be expressed in the form of the impulse response function (Green's function) [35]:

$$\begin{cases} u_t(x,t) - ku_{xx}(x,t) = 0 & (x,t) \in \mathbb{R}\times(0,\infty) \\ u(x,0) = \delta(x) \end{cases} \qquad (3\text{-}9)$$

17

where $\delta(x)$ is the Dirac delta function. After solving Equation (3-9), he basic solution of heat flux (Heat kernel)[36] can be obtained as follows:

$$\Phi(x,t) = \frac{1}{\sqrt{4\pi kt}} e^{-\frac{x^2}{4kt}}$$ (3-10)

Through Hooke's law (3-3), temperature equation (3-8) and heat flux equation(3-10), this study defines the indicators for measuring the mechanical and heat transfer capabilities of a single crystal lattice as follows:

1. Stiffness K (N/mm): The reaction force measured in the simulated compression test is divided by the given displacement to evaluate the structural support force of the lattice.

2. Initial temperature difference A (℃): The coefficient before e in the temperature drop equation (3-8). The closer it is to the given temperature difference of 100°C, the closer the equation obtained by regression from simulated data is to the analytical solution.

3. Temperature drop coefficient λα (1/s): The exponential coefficient of formula (3-8), reflecting the rate of temperature drop.

4. Temperature drop time η (s): The time required to reduce the difference ΔT between the highest temperature of the system and the lowest temperature of the system by 50%. This metric is equivalent to the coefficient λα in equation (3-8).

5. Maximum heat flux Φ_{max} (W/m^2): the highest heat flux that occurs before the system reaches thermal equilibrium. This metric is intended to serve as a material threshold to prevent heat concentration and structural softening during the process.

In finite element analysis, lattice structures often incur significant computational costs due to their small and complex geometries. Using a single lattice for testing is, on the one hand, to analyze the differences between different types of lattice in the simplest case, and on the other

hand, it is hoped that an equivalent mathematical model of a single lattice can be established to reduce the computing time required for future simulations.

The six types of lattice structures analyzed in this study were generated using nTopology[27], including body-centered cubic (BCC), diamond cubic, face-centered cubic (FCC), Kelvin cubic, Octet cubic, and Fluorite cubic. The geometric shapes of the lattices are shown in Figure 10. In addition, this study also used a solid cube REF with a side length of 1 mm to conduct the same test as a benchmark for comparing the six lattice structures.
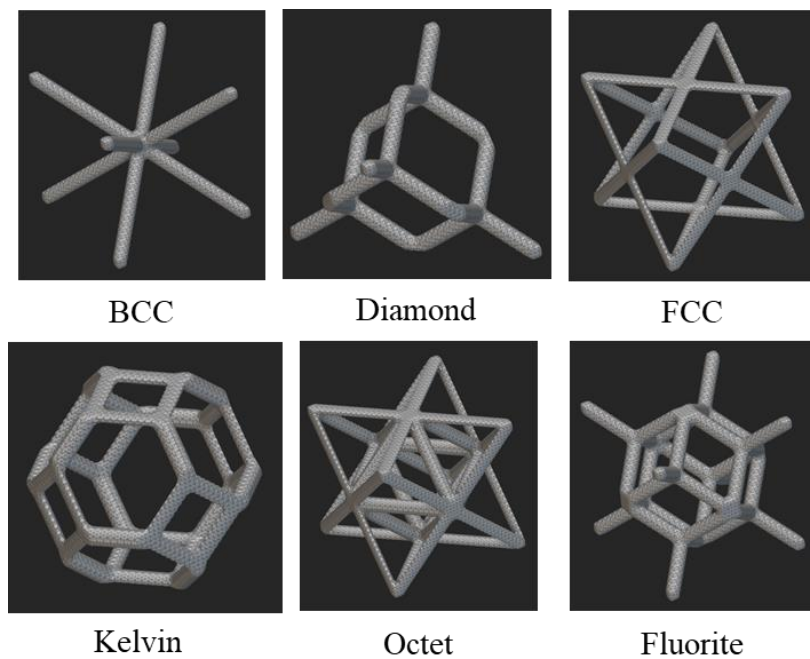
Figure 10. 6 lattice structures generated via nTopology [27]

3.2 Simple geometry test

In the manufacturing process of SLM, there have been studies on applying lattice to the support structure to prevent the workpiece from collapsing during the printing process. However, there are currently few studies that explore the influence of lattice type on simple geometries of workpiece surfaces, such as plane, inclined plane, curved surface and other structures. As can be seen from Figure 10, BCC, Diamond, and Fluorite focus on corner support,

19

while FCC, Kelvin, and Octet focus on surface support. Therefore, different lattice will have inconsistent effects on different surface geometries. If it can be discovered which lattice has the best adaptability to different workpiece geometries, it will help processors select the appropriate lattice support for individual components.

To explore the influence of six kinds of lattice structures on the geometry of SLM workpieces, this study uses a simple geometry test to establish three kinds of simple geometric structure models as processing components, including (a) a cube with a side length of 3cm; (b) A triangular column with a width of 3 cm is divided into overhang surfaces of 15°, 30°, and 45° for different slope tests; (c) A cylinder with a width of 3 cm is divided into a curvature radius of 2 cm, 3 cm, and 4 cm for different curvature tests, as shown in Figure 11. For each geometric model, six types of lattice are used as supporting structures in sequence to observe the total deformation and thermal stress effects on planes, inclined planes, and curved surfaces. This study uses Simufact Additive [37] for SLM simulation verification, and the remaining process variables are exactly the same as the boundary conditions described in Chapter 錯誤! 找不到 參照來源。.
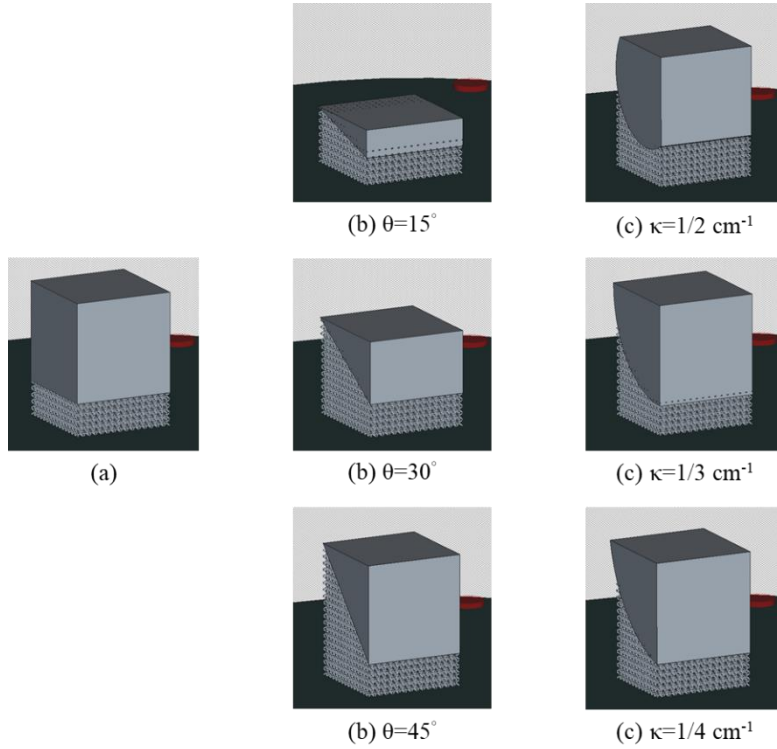
Figure 11. Simple geometry test: (a) cube, (b) triangular prism, (c) arc surface [37]

3.3 Optimization of lattice structure design parameters

In the SLM workflow, workpieces are manufactured layer by layer, so support structures are often needed to prevent the workpiece from collapsing during the printing process. The lattice structure is an option that can be used as a support structure in SLM because it can maintain rigidity and provide support while reducing material consumption, complementing metal additive manufacturing. In recent years, how to use support structures to perform heat dissipation functions to reduce thermal deformation while meeting rigidity and providing support has become a research direction that has attracted much attention. However, most current studies only explore the mechanical properties such as the rigidity of the lattice structure, but rarely analyze the heat transfer capability of the lattice structure. Therefore, this study uses the full factorial design method to explore the influence of three design parameters: lattice type, cell size, and strut diameter on the thermal deformation of the femoral component, to provide processors with the best lattice structure design parameters to reduce the thermal deformation

of SLM finished products.

Before generating the support structure, it is necessary to determine the printing direction of the workpiece. A good printing direction can minimize the support structure volume and printing time, and even eliminate overhang areas. However, in most cases, the overhang area of complex geometric workpieces is unavoidable. At this time, it is necessary to fill the overhang area with a support structure to prevent the workpiece from collapsing during the printing process. The current overhang determination method mainly uses the maximum supporting angle to identify the overhang area, and its formula is shown in Equation (3-11)

$$n \cdot d \leq -\cos(\alpha_{\max})$$
(3-11)

where n is the normal vector of the overhanging surface; d is the printing direction; $\alpha_{\max}$ is the maximum supporting angle, which the critical angle within the AM limit that can maintain the overhang structure from collapsing. The critical overhang angle is usually determined by the properties of the metal powder itself, but generally speaking, this angle is usually preset to 45 ° and is used by most commercial software. The colored area in Figure 12 is the identification result of the hanging area of the femoral component by Simufact Additive simulation software[37].
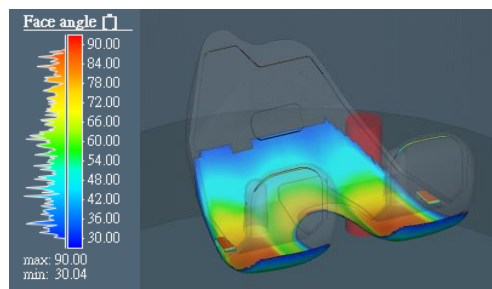
Figure 12. Femoral overhang area identification

Project the overhang area vertically onto the base plate, and the resulting space is where the support structure needs to be filled. To fill in the lattice unit, the space under the overhang area of the femoral component needs to be transformed into a voxel grid. This step is called voxelization. The result of using Matlab is shown in Figure 13. The result of voxelization is a

22

3-dimensional grid array, which contains pixels and coordinates information with values of either 0 or 1. If the pixel value at a certain coordinate is 0, it means that there is no material there. If the pixel value at a certain coordinate is 1, it indicates that there is substance. Through the voxelization results, the lattice units can be filled in the overhang areas that need support according to the coordinate information, and the lattice support structure can be generated in a stacked manner. In the mathematical model of periodic crystal structure [38], any lattice point is described by the position and vector of its lattice point, as shown in Equation (3-12):

$$r = \sum n_i a_i \qquad\qquad (\text{ 3-12 })$$

where n_i is the lattice unit integer; a_i is the unit vector along the principal crystal direction; i is the number of crystal corners.

This study uses the 6 types of lattice structures shown in Figure 10 to establish the support structure, and the stacking results according to the voxelization of the overhang area are shown in Figure 14.
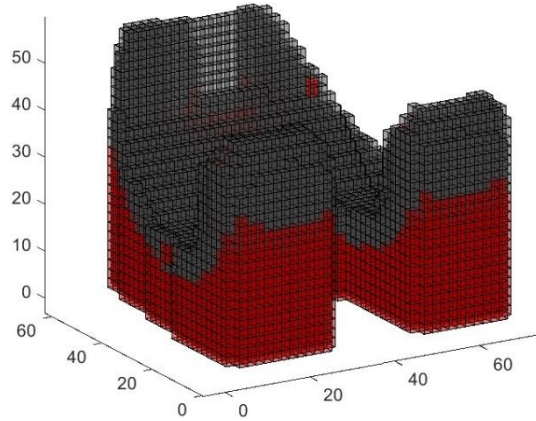
Figure 13. Voxelization of femoral component overhang areas
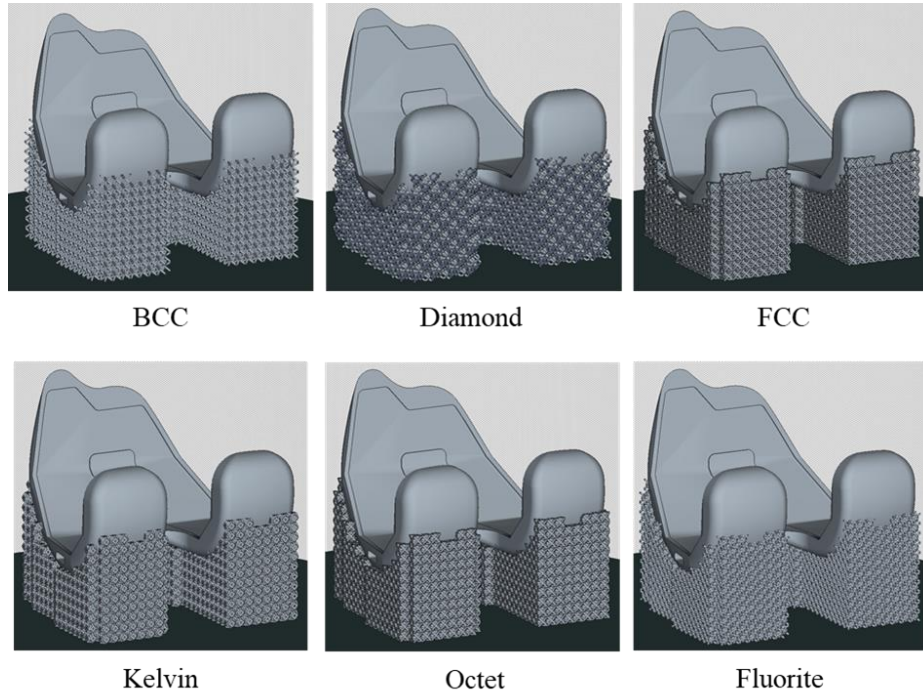
Figure 14. 6 types of lattice support structures based on overhang areas

The geometry of the lattice structure is determined by two parameters: cell size and wall thickness. To facilitate the calculation of the cross-sectional area during heat transfer, the strut diameter in the lattice is equivalent to the wall thickness. Relative density is also a common parameter to measure the lattice structure. Here the relative density is determined by the thickness of the lattice wall and is the strain of the wall thickness. To explore the influence of the three parameters of lattice type, cell size and strut diameter on the thermal deformation of SLM bone finished products, this study used the full factorial design method to establish 24 groups of working conditions to find the optimal design parameters suitable for SLM support structures. The full factorial parameter design is shown in Table 1.

Table 1. Full factorial parameter design of lattice structure

Cell Type	Cell Size [mm]	Strut Diameter [mm]	Relative Density [%]
BCC	2	0.2	17.68
		0.3	35.51
	3	0.2	17.68
		0.3	35.51

Diamond	2	0.2	16.99
		0.3	33.13
	3	0.2	16.99
		0.3	33.13
FCC	2	0.2	21.05
		0.3	41.37
	3	0.2	21.05
		0.3	41.37
Kelvin	2	0.2	20.36
		0.3	39.40
	3	0.2	20.36
		0.3	39.40
Octet	2	0.2	36.90
		0.3	67.60
	3	0.2	36.90
		0.3	67.60
Fluorite	2	0.2	31.53
		0.3	58.00
	3	0.2	31.53
		0.3	58.00

This study used Simufact Additive [37] for SLM simulation verification. In order to ensure that the thermal deformation results of the femoral component are affected by the lattice design parameters, the other process variables need to be controlled. The laser printing parameters are shown in

Table 2, whose details are as follows: laser power (P) is 200W, scanning speed (V) is 1000mm/s, laser absorption rate is 25%, spot diameter is 100μm, powder layer thickness is 30μm, the recoating time is 10 seconds, and the Uni-directional laser scanning path is used (as shown in Figure 15). The setting conditions of the laser scanning are as shown in Table 3: the scanning width (Sw) is 5mm, there is no scanning overlap range (So), the hatching distance (Hd) is 0.07mm and there is no pause time (Tp). The metal powder material used is 316L Stainless Steel. The initial temperatures of the machine chamber, powder, and base plate during the

printing process are shown in Table 4. The heat transfer coefficients of the printing model and

base plate during the printing process and post-processing are shown in Table 5.
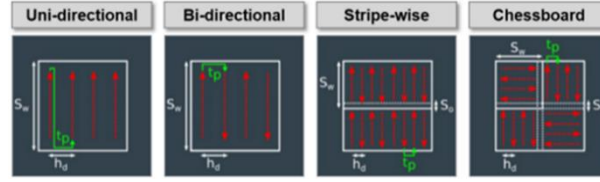
Figure 15. Scanning Strategy [37]

Table 2. Laser printing parameters

Laser power (P)	200 W
Laser speed (V)	1000 mm/s
Efficiency	25%
Beam width	100 μm
Layer thickness	30 μm
Recoater time	10 Sec

Table 3. Scanning strategy parameters

Scan width (S_w)	20 mm
Scan overlap (S_o)	0 mm
Hatch distance (H_d)	0.07 mm
Pause time (T_p)	0 Sec

Table 4. Ambient temperature parameters

Powder temperature	25°C
Chamber temperature	50°C

Initial Base Temperature	200°C

Table 5. Heat transfer coefficient of the workpiece and baseplate

Units: W/m^2-K

Model/Supporting structure		
Condition	Pre-processing	Post-processing
Emissivity	0.85	0.6
Heat transfer coefficient	12	20
Baseplate		
Condition	Pre-processing	Post-processing
Emissivity	0.6	0.6
Heat transfer coefficient	20	20
Contact HTC	100	100

Parametric effect analysis

4.1 Analysis of thermal properties of single crystal lattice

In order to prove the effectiveness of the single lattice sandwich method, this study first tested the effectiveness of interlayers with different lattice numbers. The most common BCC was selected as the lattice type to be verified. The lattice numbers are square arrays of 1×1, 3×3, and 5×5 respectively, and the boundary conditions described in Chapter 3.1 are applied. The temperature drops and heat flux obtained by numerical simulation are shown in Figure 16 to Figure 21. The comparison of the maximum temperature decrease trend line in the three cases is shown in Figure 22, and the comparison of the maximum heat flux decrease trend line is shown in Figure 23. It can be seen from the trend chart that the temperature drop curves of the three lattice arrays almost completely overlap, and the heat flux drop curve will increase slightly as the number of lattices increases. It can be seen that when the lattice structure is repeatedly arranged, the temperature decrease trend will not be affected by changes in the number of horizontal arrays, but only by the thickness of the vertical interlayers, which is consistent with the theoretical heat conduction formula (3-1); and a slight increase in heat flux may Heat conduction from the horizontal direction means heat conduction at the contact surface between lattice and lattice. Through the above results, it can be ensured that the validity of a single lattice analysis is sufficient to reflect the thermal behavior of interlayers with different lattice numbers.
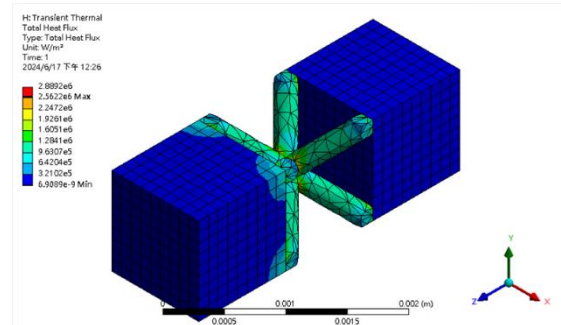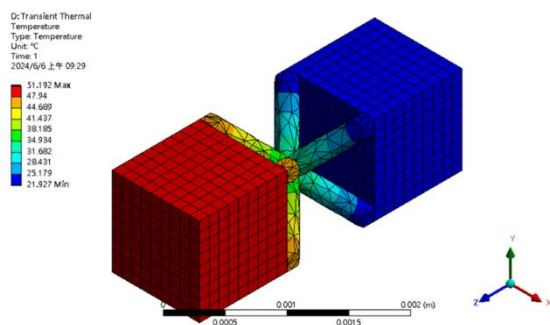
Figure 16. BCC 1×1 temperature drops
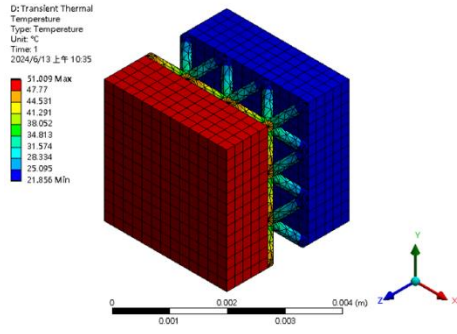
Figure 17. BCC 1×1 heat flux
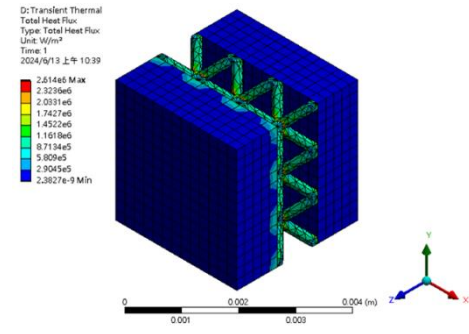
Figure 18. BCC 3×3 temperature drops
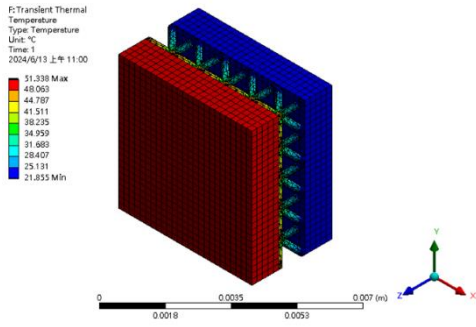
Figure 19. BCC 3×3 heat flux
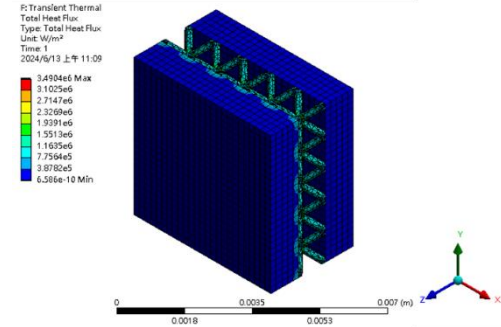
Figure 20. BCC 5×5 temperature drops
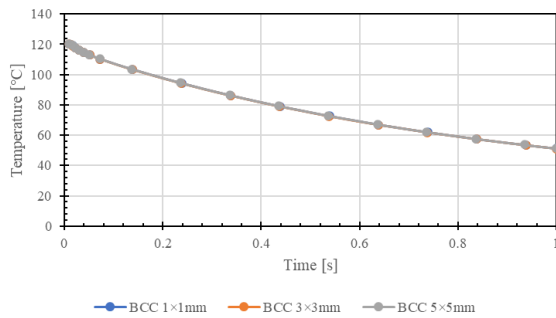
Figure 21. BCC 5×5 heat flux
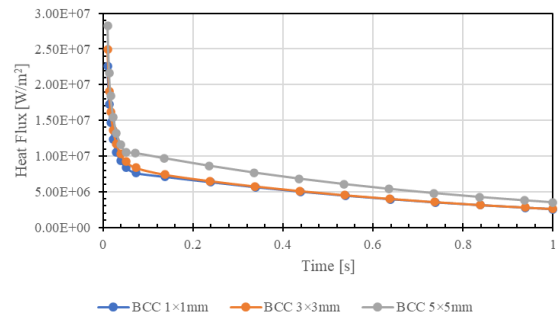
Figure 22. BCC Comparison of temperature drops with different numbers of lattice

Figure 23. BCC Comparison of heat fluxes with different numbers of lattice

To compare the mechanical properties of lattice structures, this study uses compression tests to calculate the stiffness of a single lattice to measure the load-bearing capacity of the lattice when used as an SLM support structure. Using the boundary conditions defined in Chapter 3.1 to conduct simulation tests using Ansys 2020 R1, the obtained single lattice stiffness is BCC's K=2152.5N/mm, FCC's K=18316N/mm, and Kelvin's K=8397.5N/mm, Octet's K=24393N/mm, Fluorite's K=12776N/mm, Diamond's K=3812.2N/mm, their rigidity

comparison is shown in Figure 24. Considering that the femoral component weighs 262 grams, the lattice structure can fully provide the support required in the SLM process.
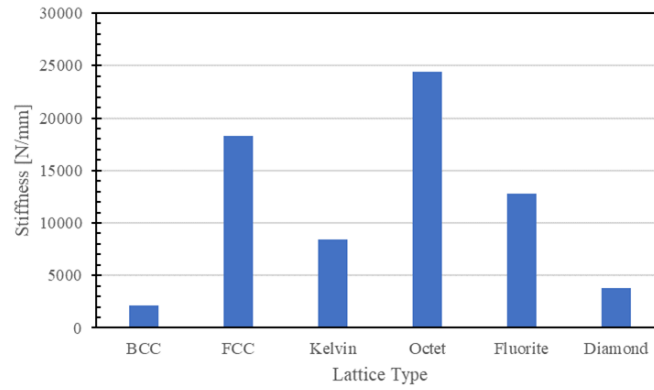
Figure 24. Single lattice stiffness comparison

To compare the thermal effects of lattice structure types, this study proposes a sandwich method and defines two indicators, the temperature drop time η and the maximum heat flux Φ_{max}, to quantify and analyze the heat transfer performance of the lattice structure. Using Ansys 2020 R1 to conduct simulation tests using the boundary conditions defined in Chapter 3.1, the single lattice temperature drop time obtained is: BCC's $\eta = 0.547$s, FCC's $\eta = 0.334$s, Kelvin's $\eta = 0.412$s, Octet's $\eta = 0.256$s, Fluorite's $\eta = 0.271$s, and Diamond's $\eta = 0.523$s. The temperature drop simulation diagrams and cooling trend diagrams are shown in Figure 25 to Figure 36. In addition, this study also compared the temperature drop curves of the solid cubic REF as the interlayer and six lattice structures and concluded that the order of cooling capabilities from strong to weak is Octet > Fluorite > Kelvin > FCC > Diamond > BCC, as shown in Figure 37.
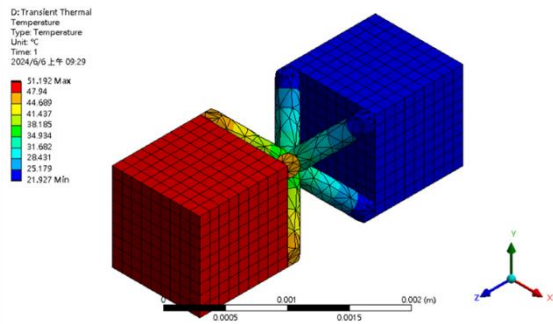
Figure 25. BCC Temperature drops
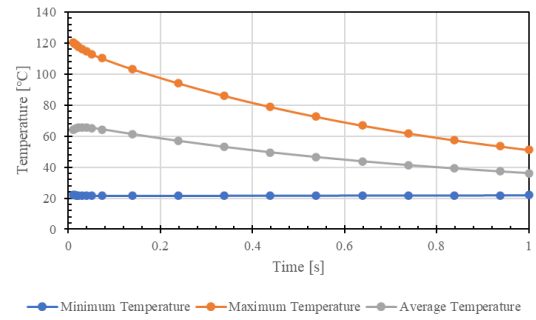
Figure 26. BCC Temperature drop trend
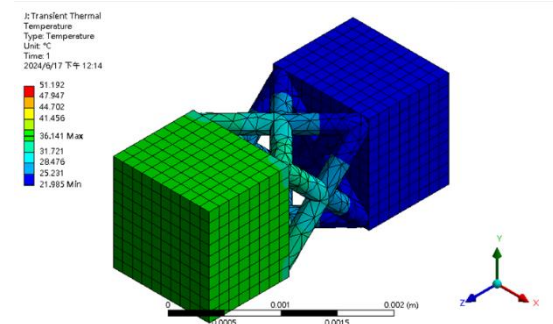
chart

Figure 27. FCC Temperature drops
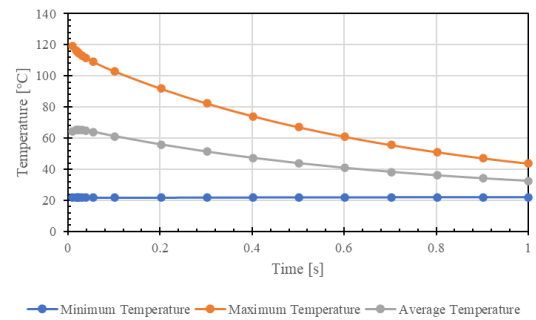
Figure 28. FCC Temperature drop trend
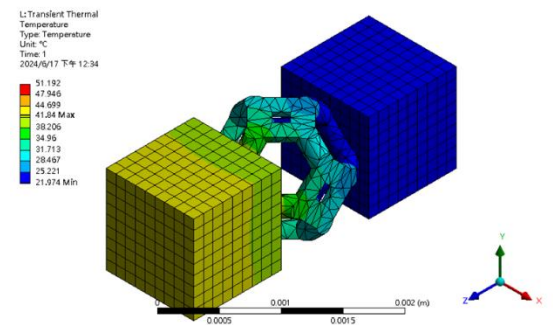
chart

Figure 29. Kelvin Temperature drops
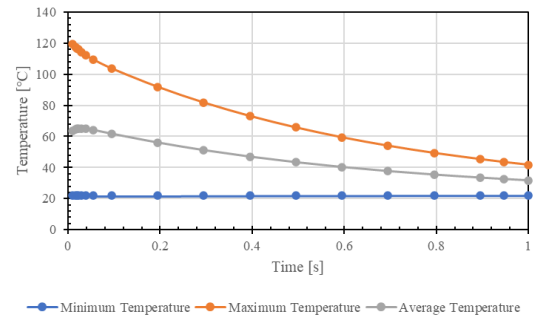
Figure 30. Kelvin Temperature drop trend
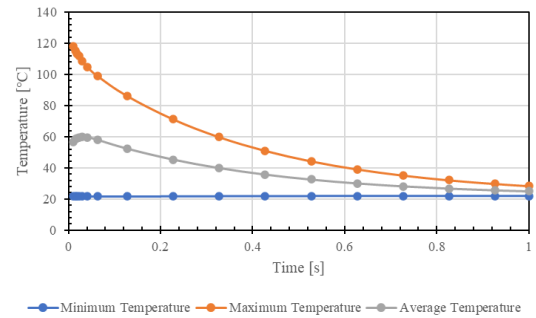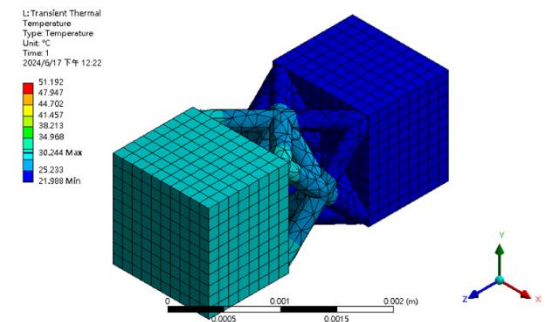
chart

Figure 31. Octet Temperature drops
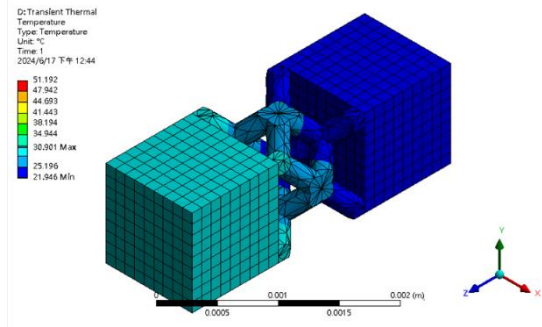
Figure 32. Octet Temperature drop trend chart
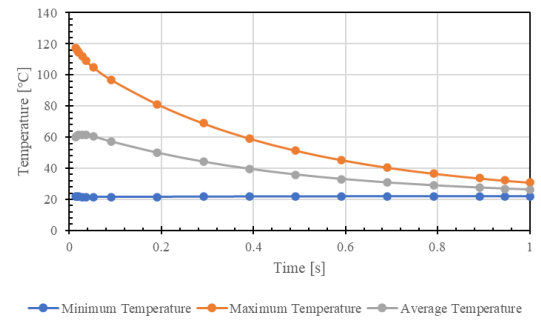
Figure 33. Fluorite Temperature drops
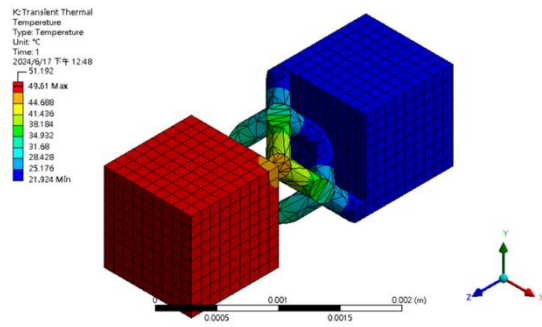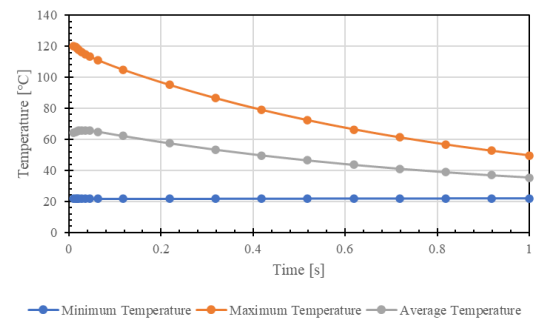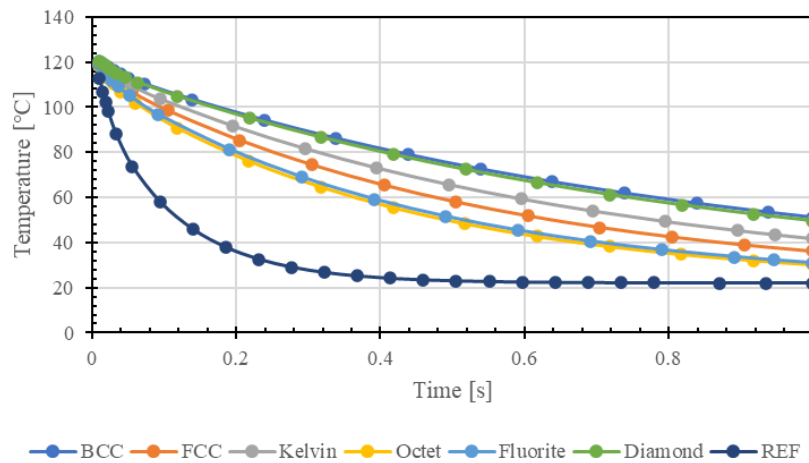

Figure 34. Fluorite Temperature drop trend chart

Figure 35. Diamond Temperature drops

Figure 36. Diamond Temperature drop trend chart

Figure 37. Comparison chart of the decreasing trend of the maximum temperature of single lattices

The maximum heat flux of a single crystal lattice during the cooling process is: BCC's Φ_{max} = 2.26×10^{7}W, FCC's Φ_{max} = 1.96×10^{7}W, Kelvin's Φ_{max} = 2.44×10^{7}W, Octet's Φ_{max} = 1.61×10^{7}W, Fluorite's Φ_{max} = 2.22 ×10^{7}W, Diamond's Φ_{max} = 2.78×10^{7}W, its heat flux simulation diagram and heat flux trend diagram are shown in Figure 38 to Figure 49. In addition, this study also compared the heat flux decline curves of the solid cube REF as the interlayer and the six lattice structures and concluded that the heat concentration effect was ranked from high to low as Diamond > Kelvin > BCC > Fluorite > FCC > Octet, as shown in Figure 50.

According to the temperature drop equation (3-8) and the thermal gradient equation (3-10), this study regresses the above data into an exponential trend line, and the equation coefficients are summarized in Table 6. Through the metrics, the heat transfer capability of each lattice can be easily evaluated, allowing the processor to select the best lattice structure according to the use situation. In addition, it is also possible to propose a mathematical equivalent model of a single lattice to significantly simplify the computational cost of simulations in finite elements.
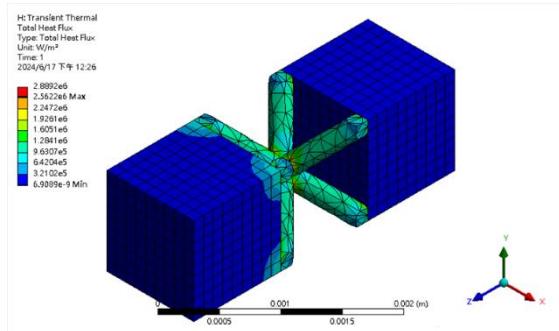
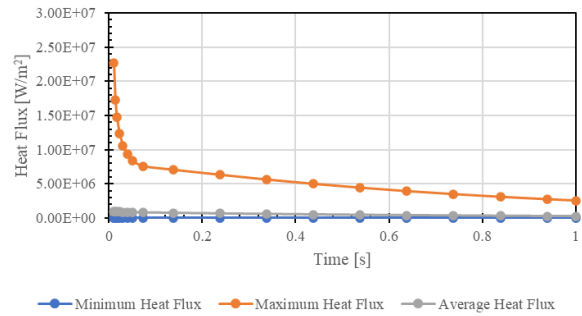Figure 38. BCC heat flux

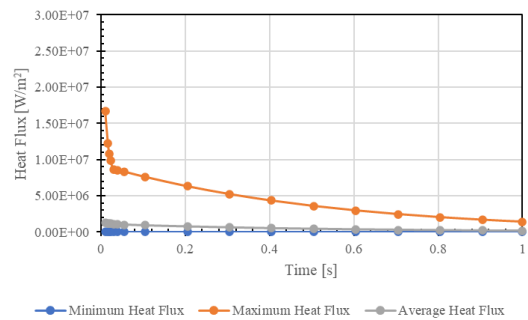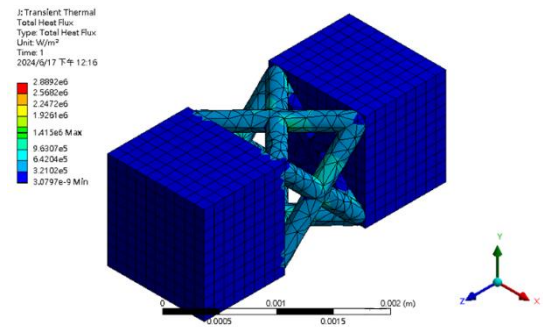Figure 39. BCC heat flux trend chart
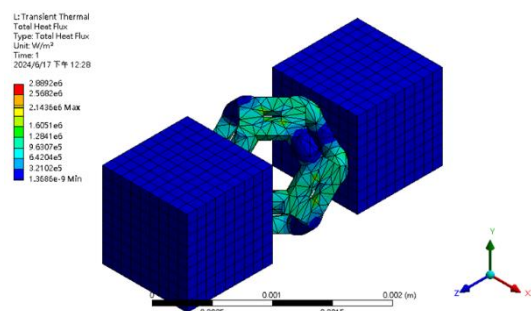
Figure 40. FCC heat flux
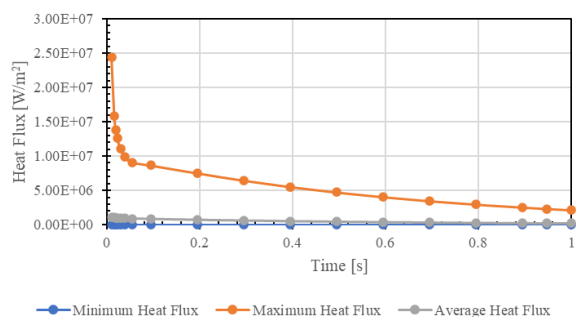

Figure 41. FCC heat flux trend chart
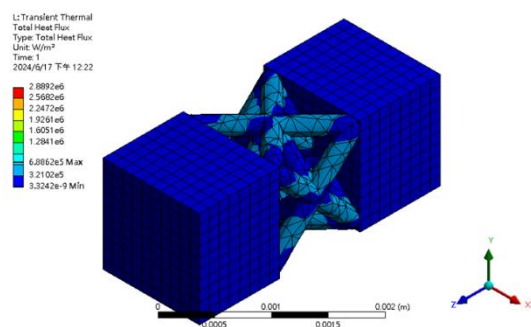

Figure 42. Kelvin heat flux

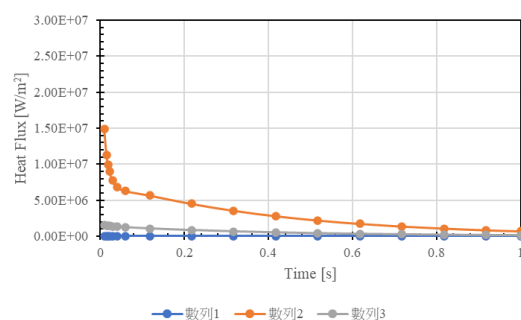Figure 43. Kelvin heat flux trend chart

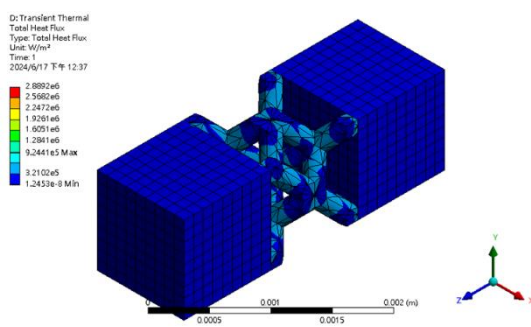Figure 44. Octet heat flux

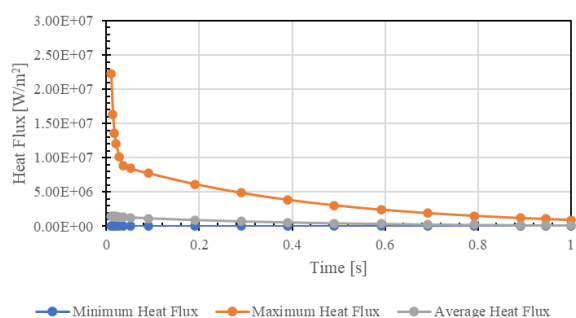
Figure 45. Octet heat flux trend chart
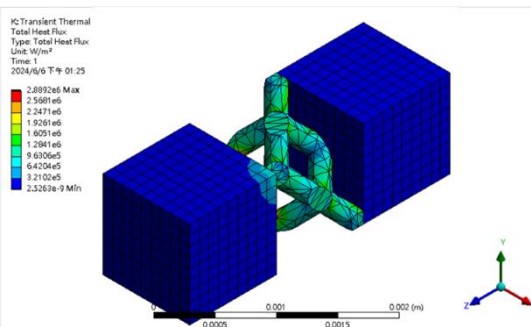

Figure 46. Fluorite heat flux
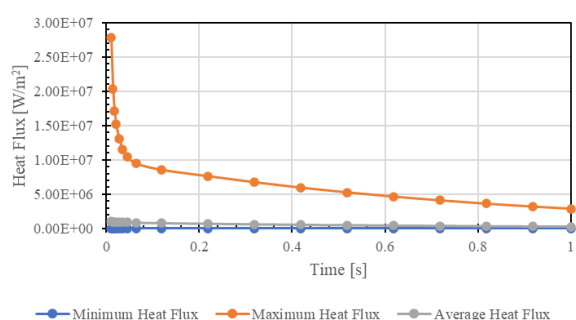

Figure 47. Fluorite heat flux trend chart

Figure 48. Diamond heat flux

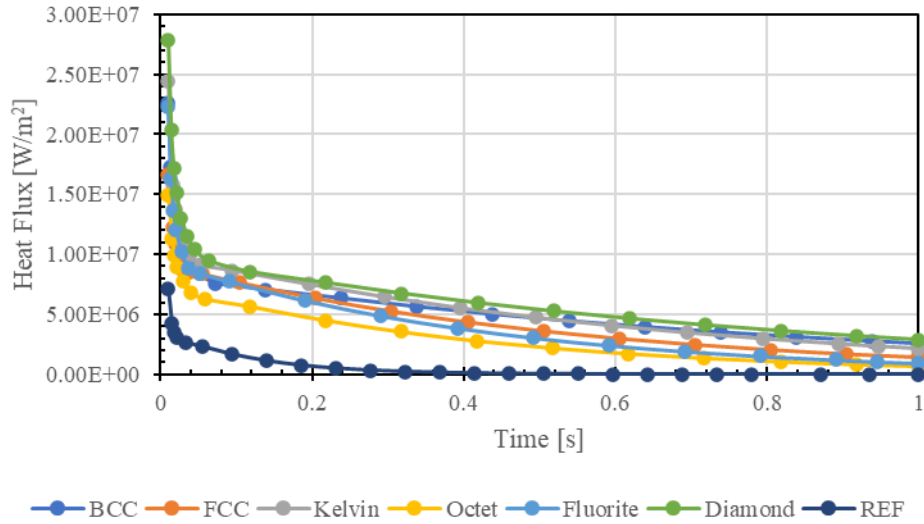Figure 49. Diamond heat flux trend chart

Figure 50. Comparison chart of the decreasing trend of the maximum heat flux of single lattices

Although all 6 types of lattice structures can provide sufficient support, in practical applications it is still desirable to select a higher rigidity lattice to reduce deformation as much as possible. In order to optimize the heat dissipation capacity, the temperature drop time should be as low as possible, which means that the lattice can quickly achieve system cooling through heat conduction; the maximum heat flux during the process should be as low as possible, which means that the lattice is concentrated due to heat during the heat dissipation process. The risk of structural softening and failure is lower. Based on the above, Octet should have the best mechanical and heat transfer performance among the 6 lattice structures. The reasons are due to its higher structural rigidity, higher relative density, which reduces the heat energy absorbed per unit volume, and its higher cross-sectional area. Improved thermal conductivity.

Table 6. Summary of single lattice rigidity, temperature drop and heat flux metrics

Cell Type	Stiffness	Temperature drop			Heat flux
	K [N/mm]	A [°C]	$\lambda\alpha$ [1/s]	η [s]	Φ_{max} [W/m^2]
BCC	2152.5	97.95	1.227	0.5475	2.262×10^7
FCC	18316	96.11	1.959	0.3343	1.668×10^7
Kelvin	8397.5	96.86	1.605	0.4124	2.438×10^7
Octet	24393	95.72	2.536	0.2563	1.488×10^7

35

Fluorite	12776	96.75	2.449	0.2713	2.224×10^7
Diamond	3812.2	97.89	1.284	0.5235	2.780×10^7
REF	206230	97.04	10.29	0.0644	0.714×10^7

4.2 Lattice support effect of simple geometry

In order to explore the influence of lattice types on workpiece surface geometry in SLM, this study uses six types of lattices as support structures for cubes, triangular prisms, and arc surfaces to compare the total displacement and thermal stress effects after printing. The first is a cube with a side length of 3 cm, and the 8 corners of the cube are used as 8 monitoring points, as shown in Figure 51. The total displacement results of the cube after printing show that the overall displacement shows a decreasing trend with the higher number of layers. The displacement of the top surface (Node 1~4) has a high degree of overlap, and the displacement of the bottom surface (Node 5~8) is consistent with the support structure. The contact part varies depending on the lattice type, as shown in Figure 52 and Figure 53. Comparing the lattice support types, the order of average displacement from low to high is Fluorite < Octet < BCC < Kelvin < FCC < Diamond. The thermal stress results of the cube after printing show that the overall stress also shows a decreasing trend as the number of layers increases, and the stress concentration is located where the bottom surface contacts the support structure. It is necessary to guard against warping or detachment, as shown in Figure 54 and Figure 55. It is worth noting that the Diamond lattice is mirror-arranged with its adjacent lattice in the array, resulting in staggered and uneven stress results. Therefore, it is not recommended to use this lattice support plane. Comparing the lattice support types, the order of average thermal stress from low to high is Diamond < Kelvin < FCC < BCC < Octet < Fluorite. To sum up the above, in the case of horizontal plane geometric elements, the ordering of total displacement and thermal stress by lattice type shows almost opposite trends. The reason for this non-compliance with Hooke's law may be due to the difference in structural rigidity caused by the relative density of the lattice,

and this difference is enough to reverse the printing results. Therefore, when choosing a lattice type, there is a trade-off between reducing total displacement and preventing warpage caused by residual stress.
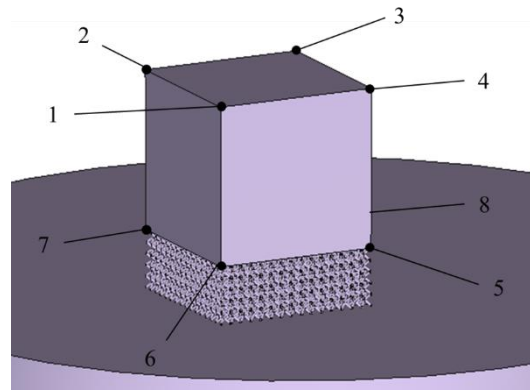

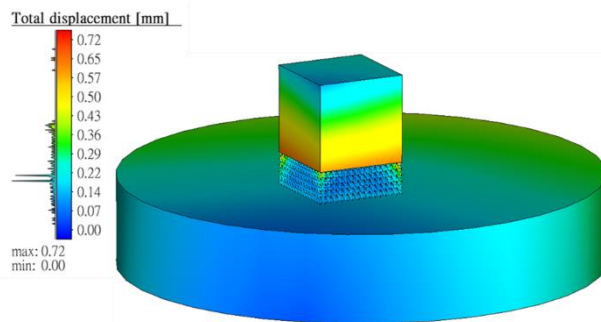Figure 51. The monitoring points of the cube

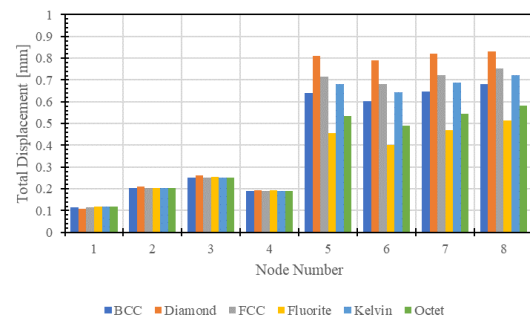
Figure 52. The total displacement of the cube

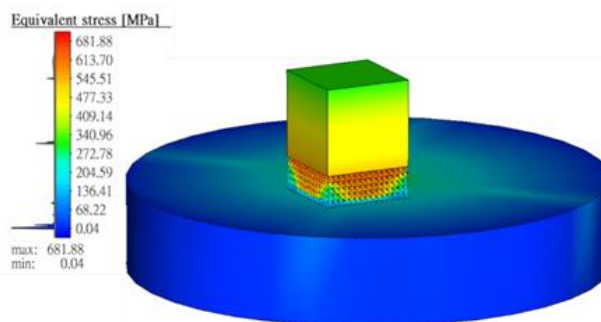Figure 53. Total displacement trend chart of the cube
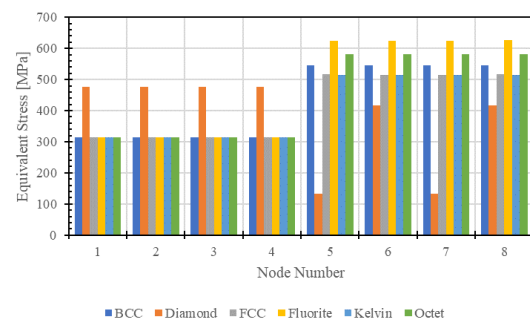

Figure 54. The thermal stress of the cube

Figure 55. Thermal stress trend chart of the cube

The second model is a triangular pillar with a width of 3 cm. Three cases of inclined plane overhang angles of 15°, 30°, and 45° are discussed respectively, and the six corners of the triangular column are selected as six monitoring points, as shown in Figure 56. The total displacement results of the triangular pillar after printing show that the overall displacement also shows a decreasing trend with the higher number of layers. However, the displacement of the contact part between the inclined surface and the support structure decreases more slowly than the vertical surface, until the displacement at the right angle of the top surface decreases. Reduce it to the minimum, as shown in Figure 57, Figure 58, Figure 61, Figure 62, Figure 65, and Figure 66. Comparing the lattice support types, the order of average displacement from low to high is Fluorite < Octet < BCC < Kelvin < FCC < Diamond. The thermal stress results of the triangular pillar after printing show that the overall stress also shows a decreasing trend as the number of layers increases, and the stress concentration is located where the bottom surface contacts the support structure, so the risk of warping and falling off needs to be prevented, as shown in Figure 59, Figure 60, Figure 63, Figure 64, Figure 67, and Figure 68. Comparing the lattice support types, the order of average thermal stress from low to high is Fluorite < Octet < BCC < Diamond < Kelvin < FCC. In addition, comparing triangular pillar with different surface slopes, it was found that the total displacement increased slightly when the overhang angle was 30°, but the overall trend was consistent, as shown in Figure 69. Based on the above, in the case of inclined plane geometric elements, the lattice type shows a highly consistent trend in the ordering of total displacement and thermal stress, which is consistent with the prediction of Hooke's law. However, Diamond causes uneven distribution of support force and changes the order of stress due to its mirror arrangement characteristics. Therefore, it is recommended to use Fluorite as a support structure when printing components with bevels.
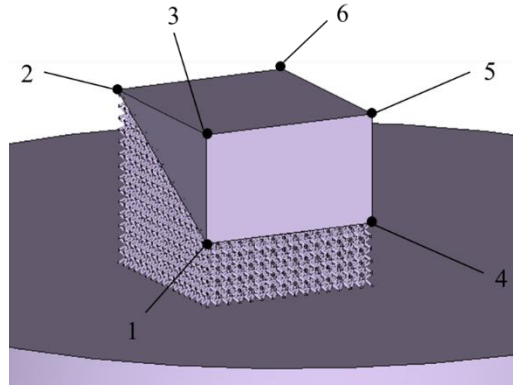
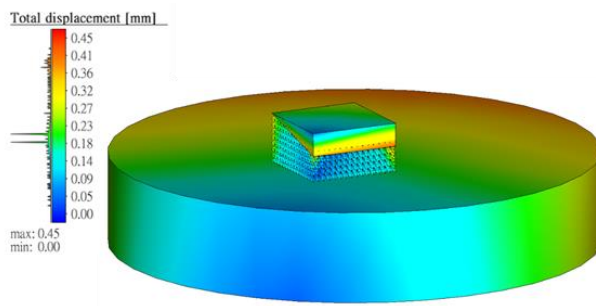Figure 56. The monitoring points of the triangular pillar

Figure 57. The total displacement of a
triangular pillar with a slope of 15°

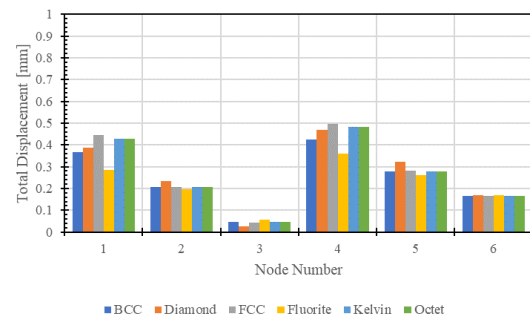Figure 58. The total displacement trend
chart of a triangular pillar with a slope of
15°

Figure 59. The thermal stress of a triangular
pillar with a slope of 15°

Figure 60. The thermal stress trend chart
of a triangular prism with a slope of 15°

Figure 61. The total displacement of a
triangular pillar with a slope of 30°

Figure 62. The total displacement trend
chart of a triangular pillar with a slope of
30°

Figure 63. The thermal stress of a triangular
pillar with a slope of 30°

Figure 64. The thermal stress trend chart
of a triangular prism with a slope of 30°

Figure 65. The total displacement of a
triangular pillar with a slope of 45°
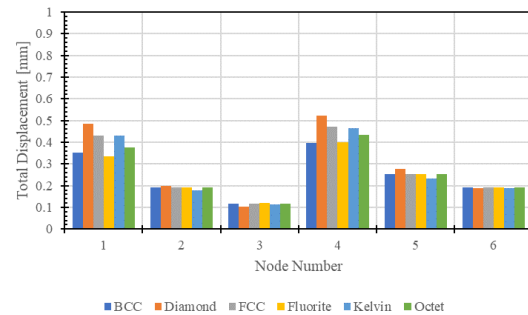
Figure 66. The total displacement trend
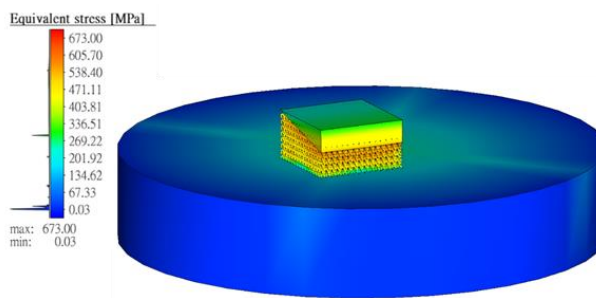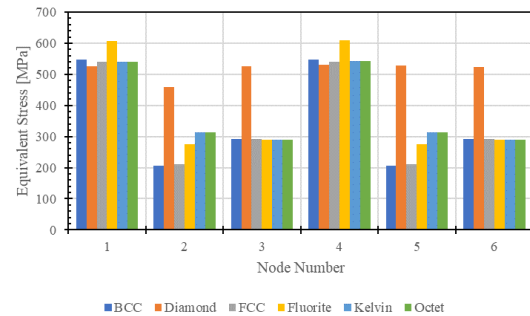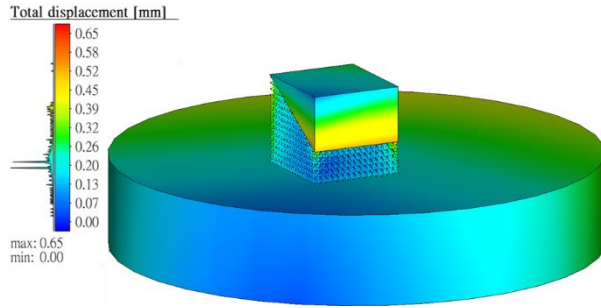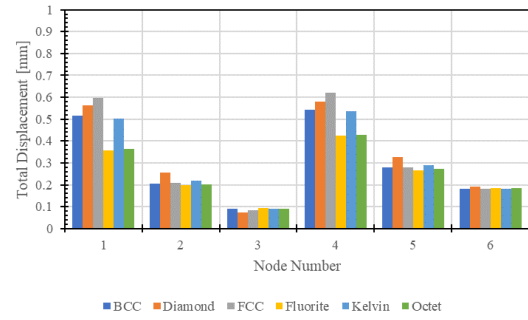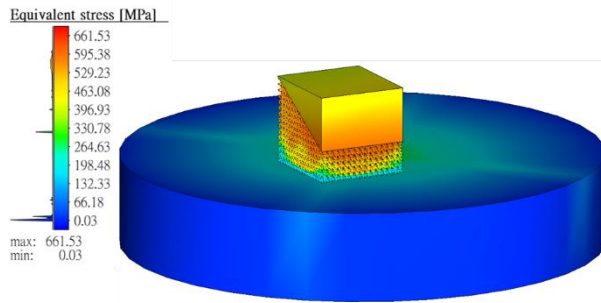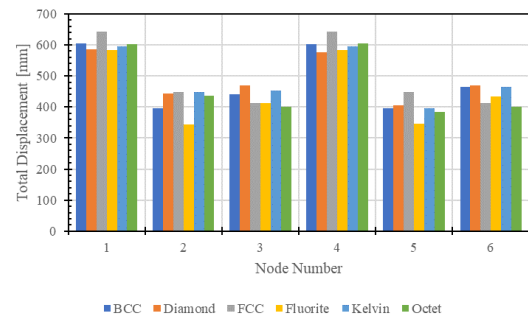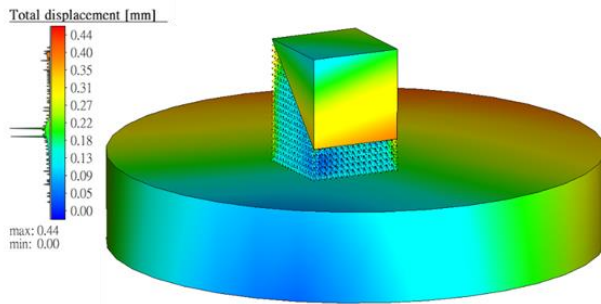chart of a triangular pillar with a slope of
45°
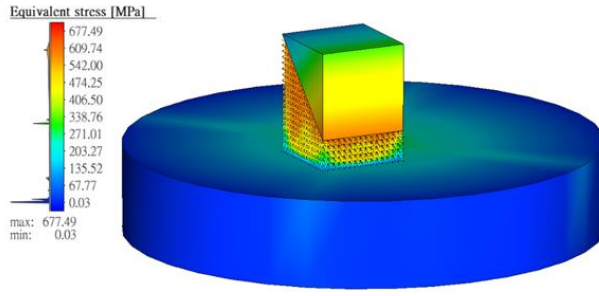
Figure 67. The thermal stress of a triangular pillar with a slope of 45°
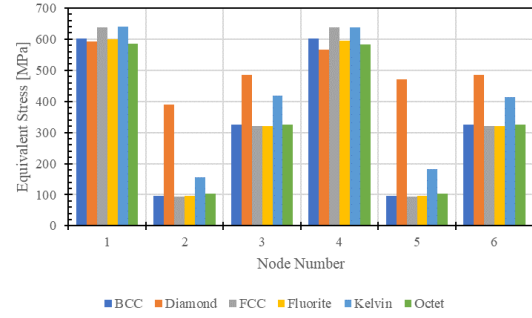
Figure 68. The thermal stress trend chart of a triangular prism with a slope of 45
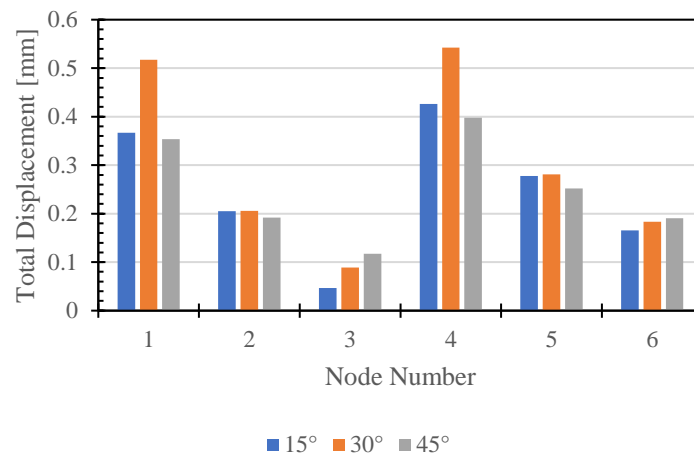
Figure 69. Comparison chart of different slopes versus total displacement

The last model is a cylinder with a thickness of 3 cm. Three cases with a curvature radius of 2 cm, 3 cm, and 4 cm are discussed respectively, and 14 nodes on the arc are selected as monitoring points, as shown in Figure 70. The total displacement results of the arc surface after printing show that the total displacement mainly changes with the angle between the printing direction and the surface normal vector. The amount of displacement has a maximum value at the bottom layer, gradually decreases to a minimum value as the angle increases to 30°, then rises back to 60° with a local maximum value, and finally decreases to a local minimum value on the top surface. The overall trend is shown in Figure 71, Figure 72, Figure 75, Figure 76, Figure 79, and Figure 80. Comparing the lattice support types, the order of average displacement from low to high is Fluorite < Octet < BCC < Kelvin < FCC < Diamond. The

thermal stress results of the arc-shaped surface after printing show that the overall stress shows a decreasing trend with higher layers. However, because the entire arc-shaped surface and the support structure are in contact with each other, the stress remains at a high value until the top. The plane has just dropped, as shown in Figure 73, Figure 74, Figure 77, Figure 78, Figure 81, and Figure 82. Comparing the lattice support types, the order of average thermal stress from low to high is Kelvin < FCC < Octet < Fluorite < BCC < Diamond. In addition, comparing cylinders with different curvature radii, it is found that the total displacement results of a curvature radius of 2 cm are not as consistent as the results of 3 cm and 4 cm, but the overall trend still shows a similar trend. It can be seen that if the curvature gradually decreases, it may be closer to the result of an inclined plane, as shown in Figure 83. Based on the above, in the case of arc surfaces, the lattice type has almost no correlation with the ranking of total displacement and thermal stress, so there is no better choice. However, comparing the total displacement results of cubes, triangular prisms, and cylinders, it can be found that the ranking of the influence of lattice type on the average displacement is highly consistent. Therefore, it is recommended to use Fluorite as the most commonly used support structure.
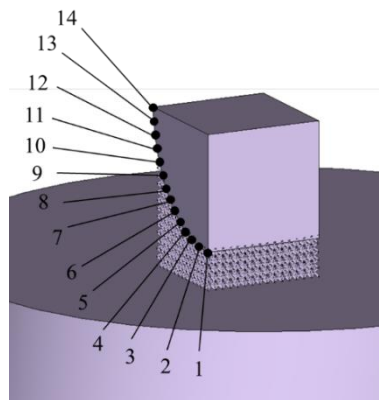
Figure 70. The monitoring points of arc surface

Figure 71. The total displacement of the cylinder with a curvature radius of 2 cm

Figure 72. The total displacement trend of the cylinder with a curvature radius of 2 cm

Figure 73. The thermal stress of the cylinder with a curvature radius of 2 cm

Figure 74. The thermal stress trend of the cylinder with a curvature radius of 2 cm
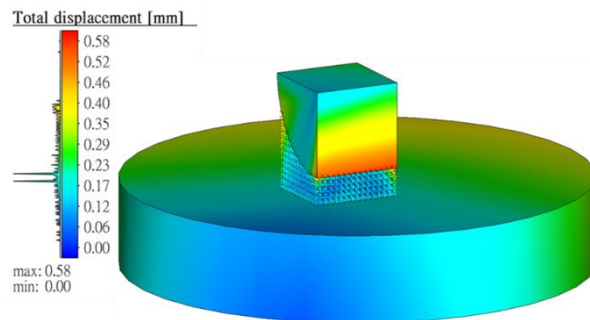
Figure 75. The total displacement of the cylinder with a curvature radius of 3 cm
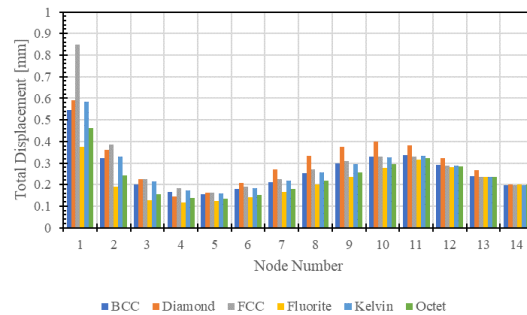
Figure 76. The total displacement trend of the cylinder with a curvature radius of 3 cm
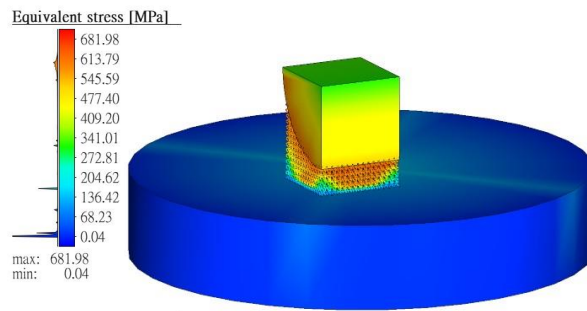
Figure 77. The thermal stress of the cylinder with a curvature radius of 3 cm

Figure 78. The thermal stress trend of the cylinder with a curvature radius of 3 cm
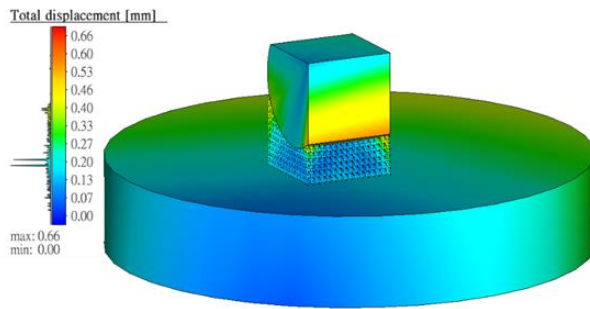

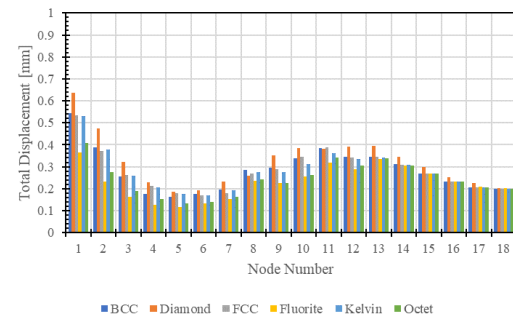Figure 79. The total displacement of the cylinder with a curvature radius of 4 cm
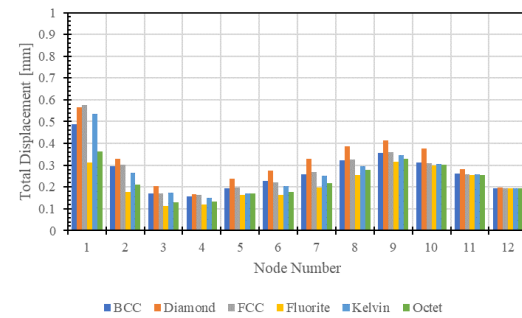
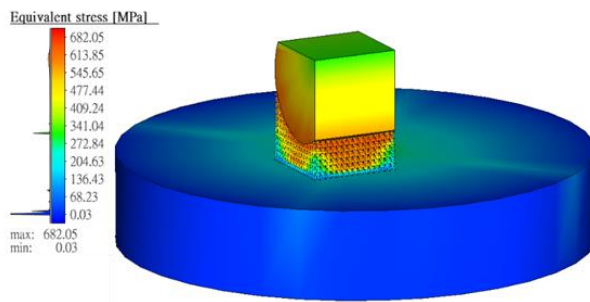Figure 80. The total displacement trend of the cylinder with a curvature radius of 4 cm

Figure 81. The thermal stress of the cylinder with a curvature radius of 4 cm
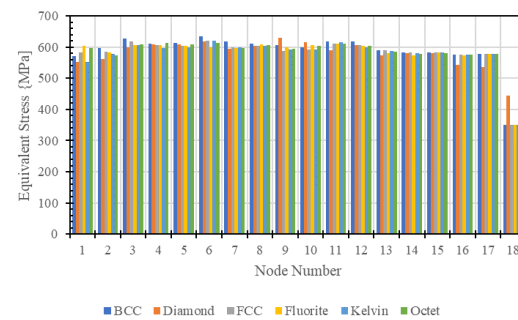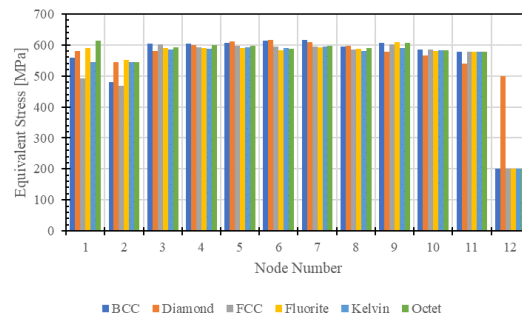

Figure 82. The thermal stress trend of the cylinder with a curvature radius of 4 cm

44
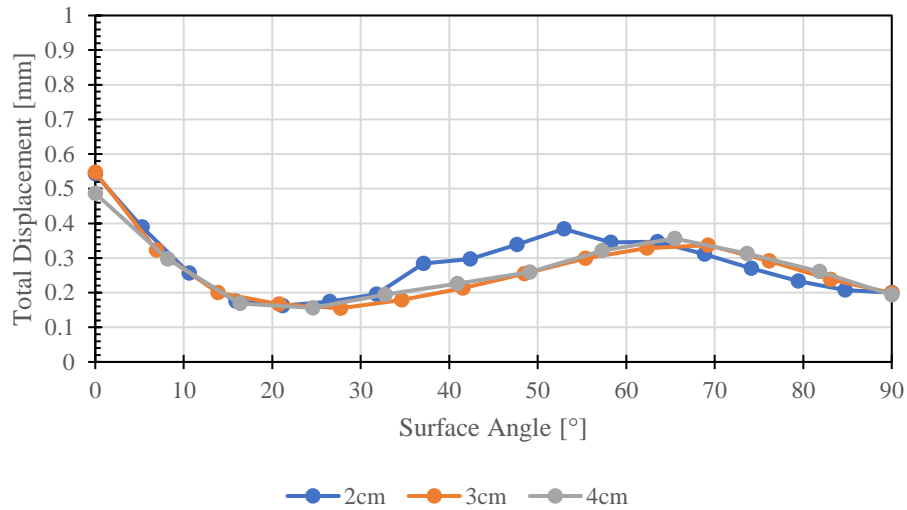
Figure 83. Comparison of total displacement of different curvature radius (the angle between the printing direction and the normal vector of the arc surface)

4.3 Effect of Lattice Support Design Parameters

To find out the optimal design parameters of the lattice support structure, this study used the full factorial design method to analyze the effects of cell size and strut diameter on the thermal deformation of SLM femoral components. 19 monitoring points were selected from the surface of the femoral component to compare the total deformation, 17 points along the native bone boundary contour, and 2 points at the tip of the nail to ensure its fit with the patient's bone, as shown in Figure 84. Under the condition of strut diameter of 0.2 mm and cell size of 2 mm, the total displacement of the femoral surface caused by different lattice support structures is shown in Figure 85, and the equivalent stress on the femoral surface is shown in Figure 86. Overall, the six types of lattice support effects are very similar, except for some differences at the right edge of the component (Node 15~17). Comparing the average values of 19 monitoring points, it is found that the average deformation values from small to large are BCC < Kelvin < FCC < Fluorite < Diamond < Octet. In Chapter 4.1, the Octet lattice has the best heat transfer capacity and has the largest deformation here. It is speculated that the reason may be that rapid

heat dissipation leads to uneven temperature distribution of the material, generating higher heat on the time scale. The gradient results in poor microstructure formation, causing the metal powders to not blend well during the melting process. This conclusion is contrary to past research ideas, which suggested reducing heat dissipation capacity in exchange for a more uniform temperature of the workpiece in the SLM process. The order of average thermal stress from small to large is Diamond < Kelvin < Octet < Fluorite < BCC < FCC, and the stress is lower in the center of the component (Node 9~11), which shows that it is easier to accumulate residual stress at the edges around the component and need to pay attention to warping and other conditions.
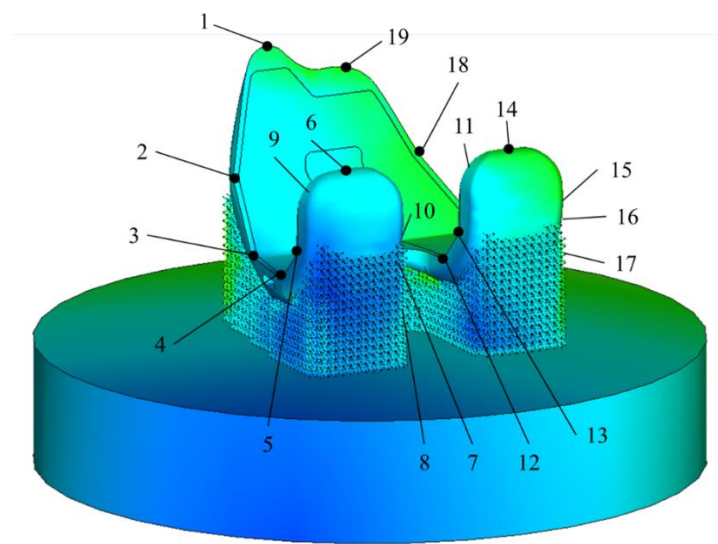
Figure 84. 19 monitoring points on the femoral surface
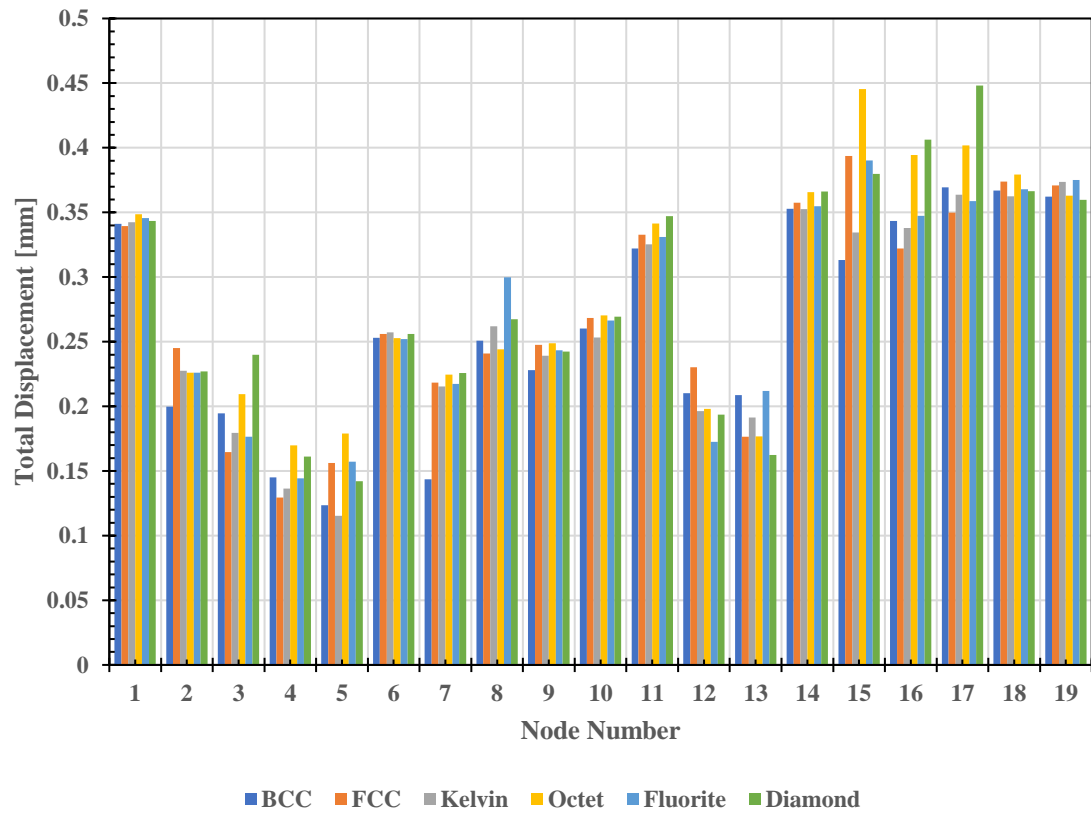
Figure 85. Comparison of the effects of 6 types of lattice supports on the total displacement
of the femoral component
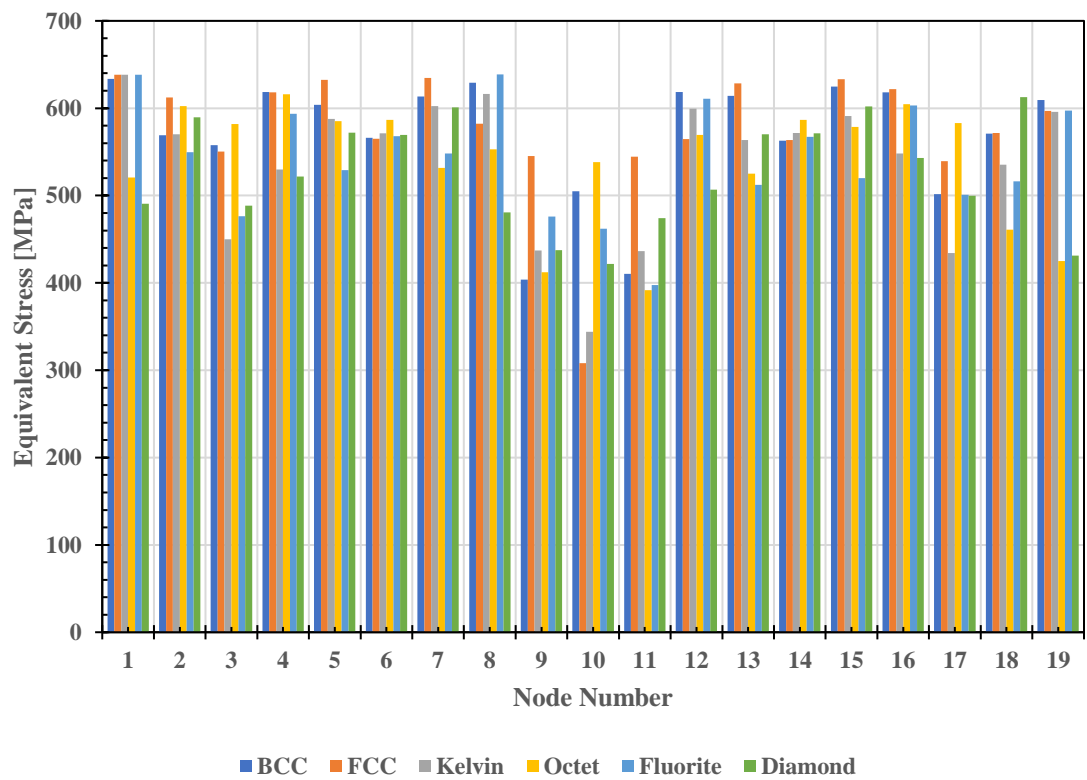
Figure 86. Comparison of the effects of 6 types of lattice supports on the equivalent stress

of the femoral component

Using the database established by the full factorial design in Table 1 in Chapter 3.3, this study uses response surface methodology (RSM) to explore the effects of the three variables of cell size, strut diameter, and relative density on total deformation, thermal stress, and thermal compliance.

First, this study averaged the total deformation of 19 monitoring points of the femoral component and then performed regression analysis on cell size-strut diameter and cell size-relative density. Since the relative density is determined by the strut diameter and the lattice type, the relative density can be regarded as the strain of the strut diameter. The regression equations of the total displacement of the femoral component are equation (4-1) and equation (4-2), and the response surface is shown in Figure 87 and Figure 88. It can be known from the response surface that strut diameter has the highest influence on the total displacement, followed by the interaction term between strut diameter and cell size, and cell size has the smallest influence. Therefore, it is recommended to reduce the strut diameter and increase the cell size to reduce the total deformation.

$$TotalDisplacement = 0.3177 - 0.0257A + 0.1298B - 0.0441AB \quad\quad (\,4\text{-}1\,)$$

$$TotalDisplacement = 0.3320 - 0.0300A + 5.2 \times 10^{-4}C - 1.9 \times 10^{-4}AC \quad\quad (\,4\text{-}2\,)$$

where A represents the cell size (mm); B represents the strut diameter (mm); C represents the relative density (%).

Figure 87. Response surface of cell size and strut diameter to total displacement

Figure 88. Response surface of cell size and relative density to total displacement

Secondly, this study averaged the thermal stress of 19 monitoring points on the femoral component and then performed regression analysis on cell size-strut diameter and cell size-relative density. The regression equations of femoral thermal stress are equation (4-3) and equation (4-4), and the response surfaces are shown in Figure 89 and Figure 90. It can be known from the response surface that increasing cell size, strut diameter, and relative density will reduce thermal stress. The trend of total displacement and thermal stress here does not seem to comply with Hooke's law. The reason may be that the relative density will change the structural rigidity rather than a constant value, and the deformation will accumulate layer by layer during the printing process.

$$EquivalentStress = 670.9381 - 42.2106A - 302.3347B - 56.4670AB \qquad (4\text{-}3)$$

$$EquivalentStress = 592.6057 - 15.1212A + 0.0786C - 0.3711AC \qquad (4\text{-}4)$$

where *A* represents the cell size (mm); *B* represents the strut diameter (mm); *C* represents the relative density (%).

Figure 89. Response surface of cell size and strut diameter to thermal stress

Figure 90. Response surface of cell size and relative density to thermal stress

Finally, this study performed a regression analysis of thermal compliance on cell size-strut diameter and cell size-relative density respectively. The physical definition of thermal compliance is the heat that a structure can absorb and mathematically is the total displacement multiplied by the thermal stress. The regression equations of thermal compliance are equation (4-5) and equation (4-6), and the response surfaces are shown in Figure 91 and Figure 92. It can be seen from the response surface that increasing the cell size can reduce the thermal compliance, while increasing the strut diameter and relative density can slightly reduce the thermal compliance.

$$ThermalCompliance = 206.5538 - 25.7890A - 12.0669B - 6.0754AB \qquad (4\text{-}5)$$

$$ThermalCompliance = 194.4036 - 21.3313A + 0.2613C - 0.1710AC \qquad (4\text{-}6)$$

where A represents the cell size (mm); B represents the strut diameter (mm); C represents the relative density (%).
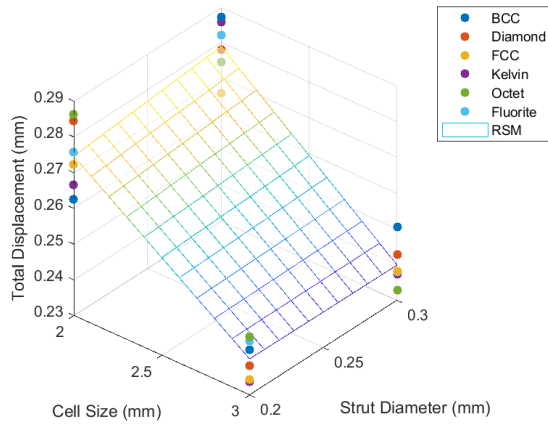
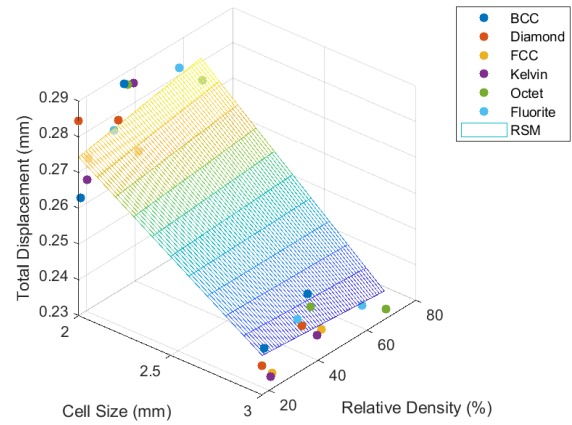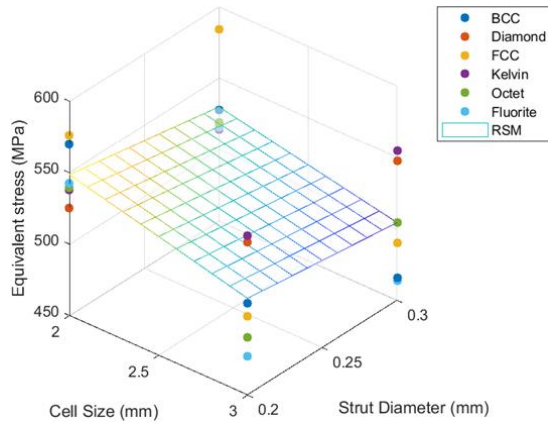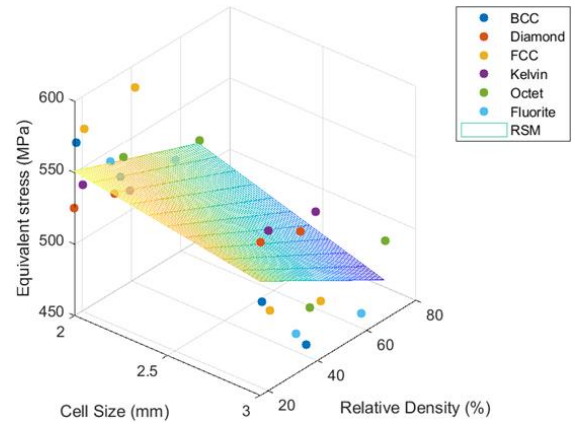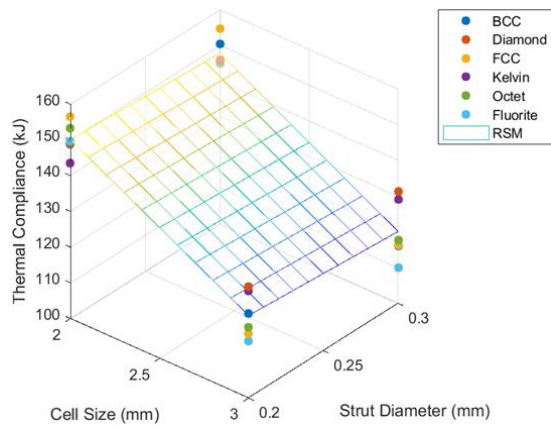Figure 91. Response surface of cell size and strut diameter to thermal compliance
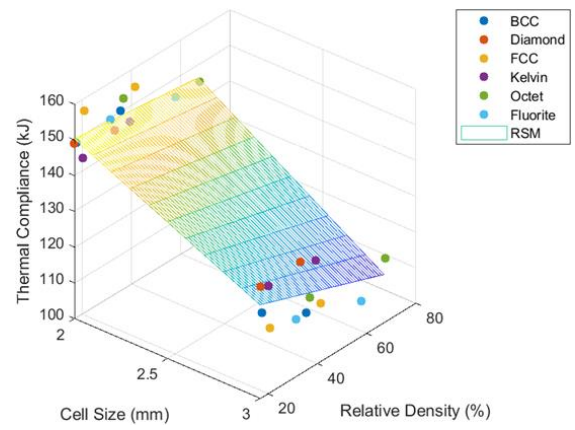
Figure 92. Response surface of cell size and relative density to thermal compliance

Discussion

5.1 Single lattice thermal properties

In this chapter, this study evaluates the thermal behavior of body-centered cubic (BCC), Diamond cubic, face-centered cubic (FCC), Kelvin cubic, Fluorite cubic, and Octet cubic through the One-lattice sandwich method as separator filling material. The two metrics of temperature drop time η and maximum heat flux Φ_{max} are defined by the basic heat conduction formula to quantify and compare the heat transfer performance of the above 6 lattice structures.

First, by comparing the horizontal arrays of BCC lattice 1×1, 3×3, and 5×5, this study found that the number of lattices in the horizontal direction does not affect the temperature decrease trend. The heat flux will be slightly increased due to horizontal heat conduction between adjacent lattice, but its impact is negligible for a single-layer lattice interlayer. Through this result, the validity of the single lattice test can be verified. However, if the number of layers in the lattice structure is greater than one, the temperature drop and heat flux may change due to thickness, but the change in heat transfer performance is predictable according to the basic heat conduction formula.

Next, this study conducted single-lattice sandwich testing on the aforementioned six lattices. Comparing the temperature drop time η, it is known that the order of cooling ability from strong to weak is Octet > Fluorite > Kelvin > FCC > Diamond > BCC; comparing the highest heat flux Φmax, it is known that the order of heat concentration risk from high to low is Diamond > Kelvin > BCC > Fluorite > FCC > Octet. The temperature drop time mainly decreases as the lattice cross-sectional area increases, while the maximum heat flux decreases as the lattice relative density increases. Based on the above results, users can sequentially select suitable lattice according to their own needs. If the user has special requirements for lattice rigidity, material consumption, etc., the lattice design parameters can also be fine-tuned to meet

the standards.

Finally, this study used solid cubic REF to replace the crystal lattice for sandwich method testing, which can compare the heat transfer performance of the above lattice structure and the solid cube. By integrating the temperature equation (3-8) and single lattice thermal performance indicators in Table 6, we can deduce the ratio of thermal resistance, thermal conductivity, and other lattice structures relative to the solid cube, and then establish a single lattice equivalent mathematical model to simplify Computational cost and complexity of modeling lattice structures in the finite element method.

5.2 Simple geometry test

In this chapter, this study designs simple geometric structures such as a cube with a side length of 3 cm, a triangular prism with overhang angles of 15°, 30°, and 45°, and a cylinder with a curvature radius of 2 cm, 3 cm, and 4 cm respectively. As SLM processing components, six types of lattice support structures are applied to evaluate the total displacement and thermal stress effects on simple geometries such as planes, inclined planes, and curved surfaces.

In the case of cubes, the total displacement shows a decreasing trend as the number of layers increases, and the deformation is largest at the contact part between the component and the support structure. The average deformation is ordered from low to high as Fluorite < Octet < BCC < Kelvin < FCC <Diamond. The thermal stress also shows a decreasing trend as the number of layers increases, and the thermal stress is also the largest at the contact part between the component and the supporting structure. The average thermal stress is ordered from low to high as Diamond < Kelvin < FCC < BCC < Octet < Fluorite. It is worth noting that the ordering of total deformation and thermal stress shows an opposite trend. The reason may be that the relative density of the lattice changes the rigidity of the supporting structure, and this effect is particularly obvious in the horizontal plane. In addition, Diamond can easily cause uneven

thermal stress distribution due to its mirror arrangement with adjacent lattice properties, so it is not recommended.

In the case of triangular pillars, the total displacement also shows a decreasing trend as the number of layers increases. However, the displacement of the contact portion between the inclined plane and the support structure decreases more slowly than the vertical plane, until the displacement at the right angle of the top plane reaches a minimum. The order of average deformation from low to high is Fluorite < Octet < BCC < Kelvin < FCC < Diamond. The overall thermal stress also shows a decreasing trend as the number of layers increases, and the stress concentration is located where the slope contacts the support structure. The average thermal stress is ordered from low to high as Fluorite < Octet < BCC < Diamond < Kelvin < FCC. Overall, the thermal performance ranking of total displacement and thermal stress shows a consistent trend, and the surface slope has little effect on the total displacement, which is consistent with the prediction of Hooke's law.

In the case of arc surfaces, the total displacement trend is closely related to the overhang angle of the arc surface. The amount of displacement has a maximum value at the bottom layer and gradually decreases to a minimum value as the overhang angle increases to 30°. Then the amount of displacement rises again until there is a local maximum value at the overhang angle of 60°, and finally decreases to a local minimum value at the top plane of 90°. The order of average deformation from low to high is Fluorite < Octet < BCC < Kelvin < FCC < Diamond. The overall thermal stress also shows a decreasing trend as the number of layers increases. However, the stress on the arc surface does not decrease significantly due to contact with the support structure. The average thermal stress is sorted from low to high as Kelvin < FCC < Octet < Fluorite < BCC < Diamond. Overall, there is no obvious correlation between the total deformation and the ordering of thermal stress. However, as the arc curvature becomes smaller, the change of the total deformation becomes slower. It is shown that in addition to the

mechanical and heat transfer properties of the lattice, the overhang angle may also be an important factor affecting the manufacturing results.

Based on the above, in the case of simple geometries such as horizontal planes, inclined planes, arc surfaces, etc., the impact of the six lattice support structures on the total deformation is almost the same, while the thermal stress has a different trend due to the interactive influence of factors such as the relative density of the lattice and the overhang angle. The deformation will decrease as the number of layers increases, and the stress will be concentrated in the contact part between the component and the supporting structure, where is needed to be careful about warping and falling off. However, residual stresses can usually be relieved by heat treatment, so Fluorite is recommended as the most common support structure.

5.3 Lattice design parameter effects

In this chapter, this study uses the full factorial design method to establish 24 groups of simulated working conditions. The response surface method was used to explore the influence of lattice type, cell size, and strut diameter among the design parameters of the lattice support structure on the total displacement, thermal stress, and thermal compliance of the SLM femoral component.

This study first uses Simufact Additive to simulate the SLM femoral component manufacturing process. With the cell size and strut diameter fixed, 19 monitoring points were selected from the femoral surface to compare the effects of six lattice structures on total deformation and thermal stress. It can be seen from the results that the total deformation and thermal stress trends produced by different lattice structures are very similar. It can be seen that various lattice types can exert almost the same support effect on the femoral component when used as a support structure without significant differences in heat dissipation capabilities. However, most of the residual stress is concentrated at the edge of the femoral component, and

you need to be careful about warping and other situations.

This study also used the response surface methodology to perform a regression analysis on the lattice design parameters and femoral component processing results. From the analysis results, it can be concluded that the cell size is negatively correlated with the total displacement, while the strut diameter and relative density have little effect on the total deformation. Increasing cell size, strut diameter, and relative density can reduce thermal stress. Increasing cell size reduces thermal compliance while increasing strut diameter and relative density slightly decreases thermal compliance. It is worth noting that changing the relative density of the lattice will also change the structural rigidity, so its solid mechanical behavior still needs further analysis. Based on the above results, it is suggested that increasing cell size can achieve a better heat dissipation effect, thereby reducing total displacement and thermal stress. However, the self-supporting limitations in the AM process should be considered when adjusting the lattice size, otherwise, the structure will collapse due to excessive lateral distance.

Conclusion

6.1 Conclusion

In the SLM processing scenario, the high-temperature gradient generated by the laser can easily cause defects such as deformation and warping of the finished product. One solution is to use a support structure to provide tension while assisting in heat dissipation. In order to explore the heat dissipation benefits of the lattice as SLM support structures, this study first proposed a single lattice sandwich method and defined two metrics: temperature drop time and maximum heat flux to quantify the heat transfer performance of the lattice structure, and then used full factorial design to explore the optimal design parameters of the lattice structure that can minimize thermal deformation of the finished SLM femoral component. The results show that Octet has the best single-lattice heat transfer performance, while Fluorite can be used as the most versatile support structure to reduce thermal deformation. Compared with solid materials, the lattice structure designed with optimal parameters can retain 50% of the thermal conductivity within a volume limit of 30%. On the premise of meeting the self-supporting limit, every 1 mm increase in cell size can reduce the average deformation of the femoral component by 0.03 mm. This research can help processors quickly evaluate the heat transfer performance of the lattice structure, and then select appropriate support structure design parameters based on the actual SLM processing situation.

6.2 Future work

In the future, the deficiencies of existing methods can still be improved and the practical application capabilities of this method can be expanded. Here are some ideas for the future:

1. Print the designed lattice support structure and measure the surface deformation of the femoral component to verify the reliability of the simulation predictions.

2. Use nonlinear regression or Physics-informed neural network (PINN) to replace the response surface method for prediction to improve the prediction accuracy of lattice parameter design to reduce thermal deformation.

3. Increase simulated data and incorporate actual measurement data to establish a database, and increase the range of input parameters and output results to establish a more general prediction system.

4. Establish a single lattice equivalent mathematical model based on quantitative heat transfer performance metrics to reduce the computational cost and complexity caused by the lattice structure in the finite element method.

Reference

[1]　人力發展統計分析圖表彙編－人口推計－國發會全球資訊網. Available at: https://www.ndc.gov.tw/Content_List.aspx?n=2688C8F5935982DC (Accessed: September 02, 2023).

[2]　翁易萱（2022）。以全表現型體關聯性研究探索共病與全人工膝關節置換術術後感染之關係。〔碩士論文。慈濟大學〕臺灣博碩士論文知識加值系統。 https://hdl.handle.net/11296/czj327。

[3]　Lin, C. M., Hung, Y. T., & Tan, C. M. (2021). Hybrid Taguchi–Gray Relation Analysis Method for Design of Metal Powder Injection-Molded Artificial Knee Joints with Optimal Powder Concentration and Volume Shrinkage. *Polymers*, 13(6), 865. https://doi.org/10.3390/polym13060865

[4]　Kebbach, M., Geier, A., Darowski, M., Krueger, S., Schilling, C., Grupp, T. M., & Bader, R. (2023). Computer-based analysis of different component positions and insert thicknesses on tibio-femoral and patello-femoral joint dynamics after cruciate-retaining total knee replacement. *The Knee*, 40, 152-165. https://doi.org/10.1016/j.knee.2022.11.010

[5]　Armstrong, M., Mehrabi, H., & Naveed, N. (2022). An overview of modern metal additive manufacturing technology. *Journal of Manufacturing Processes*, 84, 1001-1029. https://doi.org/10.1016/j.jmapro.2022.10.060

[6]　Bihr, M., Allaire, G., Betbeder-Lauque, X., Bogosel, B., Bordeu, F., & Querois, J. (2022). Part and supports optimization in metal powder bed additive manufacturing using simplified process simulation. *Computer Methods in Applied Mechanics and Engineering*, 395, 114975. https://doi.org/10.1016/j.cma.2022.114975

[7]　潘季宏（2023）。基於有限元素分析開發選擇性雷射熔融製程之熱誤差診斷網路:以人工膝關節脛骨元件為例。〔碩士論文。國立中興大學〕國立中興大學圖書館。

[8]　Yan, W., Ge, W., Qian, Y., Lin, S., Zhou, B., Liu, W. K., ... & Wagner, G. J. (2017). Multi-physics modeling of single/multiple-track defect mechanisms in electron beam selective melting. *Acta Materialia*, 134, 324-333. https://doi.org/10.1016/j.actamat.2017.05.061

[9]　Su, J., Jiang, F., Li, J., Tan, C., Xu, Z., Xie, H., ... & Teng, J. (2022). Phase transformation mechanisms, microstructural characteristics and mechanical performances of an additively manufactured Ti-6Al-4V alloy under dual-stage heat treatment. *Materials & Design*, 223, 111240. https://doi.org/10.1016/j.matdes.2022.111240

[10]　Wang, Z., Zhang, Y., Tan, S., Ding, L., & Bernard, A. (2021). Support point determination for support structure design in additive manufacturing. *Additive Manufacturing*, *47*, 102341. https://doi.org/10.1016/j.addma.2021.102341

[11]　Zhang, Y., Wang, Z., Zhang, Y., Gomes, S., & Bernard, A. (2020). Bio-inspired generative design for support structure generation and optimization in Additive Manufacturing (AM). *CIRP Annals*, 69(1), 117-120. https://doi.org/10.1016/j.cirp.2020.04.091

[12]　Zhang, N., Zhang, L.-C., Chen, Y., & Shi, Y.-S. (2019). Local Barycenter Based Efficient Tree-Support Generation for 3D Printing. *Computer-Aided Design*, 115, 277-292. https://doi.org/10.1016/j.cad.2019.06.004

[13]　Hussein, A., Hao, L., Yan, C., Everson, R., & Young, P. (2013). Advanced lattice support structures for

metal additive manufacturing. *Journal of Materials Processing Technology*, 213(7), 1019-1026. https://doi.org/10.1016/j.jmatprotec.2013.01.020

[14]   Vanek, J., Galicia, J. A. G., & Benes, B. (2014). Clever support: Efficient support structure generation for digital fabrication. *Computer graphics forum*, 33(5), 117-125. https://doi.org/10.1111/cgf.12437

[15]   Subedi, S. C., Shahba, A., Thevamaran, M., Thoma, D. J., & Suresh, K. (2022). Towards the optimal design of support structures for laser powder bed fusion-based metal additive manufacturing via thermal equivalent static loads. *Additive Manufacturing*, 57, 102956. https://doi.org/10.1016/j.addma.2022.102956

[16]   Dumas, J., Hergel, J., & Lefebvre, S. (2014). Bridging the gap: automated steady scaffoldings for 3D printing. *ACM Trans. Graph.*, 33(4), Article 98. https://doi.org/10.1145/2601097.2601153

[17]   Armanfar, A., Alper Tasmektepligil, A., Kilic, R. T., Demir, S., Cam, S., Karafi, Y., Majd, B. A. E., & Gunpinar, E. (2024). Embedding lattice structures into ship hulls for structural optimization and additive manufacturing. *Ocean Engineering*, 301, 117601. https://doi.org/10.1016/j.oceaneng.2024.117601

[18]   Longhitano, G. A., García, I. M., Arenas, M. A., de Damborenea, J. J., Maciel Filho, R., & Conde, A. (2024). Effect of designed pore size on electrochemical, wear, and tribocorrosion behavior of additively manufactured Ti-6Al-4V lattice structures. *Additive Manufacturing*, 79, 103931. https://doi.org/10.1016/j.addma.2023.103931

[19]   Han, T., Qi, D., Ma, J., & Sun, C. (2024). Generative design and mechanical properties of the lattice structures for tensile and compressive loading conditions fabricated by selective laser melting. *Mechanics of Materials*, 188, 104840. https://doi.org/10.1016/j.mechmat.2023.104840

[20]   Xu, K., Li, Y., Chen, L., & Maropoulos, P. (2024). Optimizing lightweight lattice structures through integrated parameterized design and fiber-reinforced additive manufacturing. *CIRP Annals*. https://doi.org/10.1016/j.cirp.2024.04.005

[21]   Wang, W., Feng, D., Yang, L., Li, S., & Wang, C. C. L. (2023). Topology optimization of self-supporting lattice structure. Additive Manufacturing, 67, 103507. https://doi.org/10.1016/j.addma.2023.103507

[22]   Huang, R., Dai, N., Pan, C., Yang, Y., Jiang, X., Tian, S., & Zhang, Z. (2023). Grid-tree composite support structures for lattice parts in selective laser melting. *Materials & Design*, 225, 111499. https://doi.org/10.1016/j.matdes.2022.111499

[23]   Yang, D., Pan, C., Zhou, Y., & Han, Y. (2022). Optimized design and additive manufacture of double-sided metal mirror with self-supporting lattice structure. *Materials & Design*, 219, 110759. https://doi.org/10.1016/j.matdes.2022.110759

[24]   Vaidya, R., & Anand, S. (2016). Optimum Support Structure Generation for Additive Manufacturing Using Unit Cell Structures and Support Removal Constraint. *Procedia Manufacturing*, 5, 1043-1059. https://doi.org/10.1016/j.promfg.2016.08.072

[25]   Liu, F., Chen, M., Liu, S., Xiang, Z., Huang, S., Lim, E. G., & Zhang, S. (2024). Stress-driven generative design and numerical assessment of customized additive manufactured lattice structures. *Materials & Design*, 241, 112956. https://doi.org/10.1016/j.matdes.2024.112956

[26]   Venugopal, V., Hertlein, N., & Anand, S. (2021). Multi-Material Topology Optimization Using Variable Density Lattice Structures for Additive Manufacturing. *Procedia Manufacturing*, 53, 327-337.

https://doi.org/10.1016/j.promfg.2021.06.089

[27]   nTop, nTopology Inc., retrieved from https://www.ntop.com/software/products/, accessed by June 1, 2024.

[28]   Zhuang, J.-R., Lee, Y.-T., Hsieh, W.-H., & Yang, A.-S. (2018). Determination of melt pool dimensions using DOE-FEM and RSM with process window during SLM of Ti6Al4V powder. *Optics & Laser Technology*, 103, 59-76. https://doi.org/10.1016/j.optlastec.2018.01.013

[29]   Lal Lazar, P. J., Subramanian, J., Manickam, M., & Selvaraj, V. K. (2023). Imperfections and computational modeling of lattice structures developed through powder bed fusion – A short review. Materials Today: Proceedings. https://doi.org/10.1016/j.matpr.2023.02.269

[30]   Gao, S., Ding, J., Qu, S., Liu, H., & Song, X. (2023). Numerical and experimental investigation of additively manufactured shell-lattice copper heat exchanger. International Communications in Heat and Mass Transfer, 147, 106976. https://doi.org/10.1016/j.icheatmasstransfer.2023.106976

[31]   Ferro, C. G., Pietrangelo, F., & Maggiore, P. (2023). Heat exchange performance evaluation inside a lattice panel using CFD analysis for an innovative aerospace anti-icing system. *Aerospace Science and Technology*, *141*, 108565. https://doi.org/10.1016/j.ast.2023.108565

[32]   Luo, Y., Zheng, K., Zhao, P., & Zhang, Y. (2023). Machining characteristics of 316L stainless steel in hybrid manufacturing via a three-dimensional thermal-mechanical coupled model. Journal of Manufacturing Processes, 102, 275-296. https://doi.org/10.1016/j.jmapro.2023.06.021

[33]   Hu, H., Wang, W., Ning, H., & Liu, B. (2024). Numerical simulation and experimental study on the compression performance of a double layer cross-lattice-core sandwich structure. *Structures*, 64, 106531. https://doi.org/https://doi.org/10.1016/j.istruc.2024.106531

[34]   Çengel, Y.A.. and Ghajar, A.J. (2020) *Heat and mass transfer: Fundamentals and applications*. New York: McGraw-Hill Education.

[35]   Negi, P., Cheng, M., Krishnamurthy, M., Ying, W., & Li, S. (2024). Learning domain-independent Green's function for elliptic partial differential equations. *Computer Methods in Applied Mechanics and Engineering*, 421, 116779. https://doi.org/https://doi.org/10.1016/j.cma.2024.116779

[36]   Krötz, B., Thangavelu, S., & Xu, Y. (2005). The heat kernel transform for the Heisenberg group. *Journal of Functional Analysis*, 225(2), 301-336. https://doi.org/https://doi.org/10.1016/j.jfa.2005.03.019

[37]   SimufactAdditive, MSC.SoftwareCorporation. retrieved from https://www.mscsoftware.com/product-/simufact, accessed by July 19, 2023.

[38]   Talatahari, S., Azizi, M., Tolouei, M., Talatahari, B., & Sareh, P. (2021). Crystal Structure Algorithm (CryStAl): A Metaheuristic Optimization Method. *IEEE Access*, 9, 71244-71261. https://doi.org/10.1109/ACCESS.2021.3079161

[39]   Sun, J., Yang, Y., & Wang, D. (2013). Parametric optimization of selective laser melting for forming Ti6Al4V samples by Taguchi method. *Optics & Laser Technology*, 49, 118-124. https://doi.org/10.1016/j.optlastec.2012.12.002